Accepted Manuscript

1   *MANTONIELLA BEAUFORTII* AND *MANTONIELLA BAFFINENSIS* SP.

2   NOV. (MAMIELLALES, MAMIELLOPHYCEAE),

3   TWO NEW GREEN ALGAL SPECIES FROM THE HIGH ARCTIC[1]

4   Sheree Yau[2,3]

5   Integrative Marine Biology Laboratory (BIOM), CNRS, UMR7232, Sorbonne Université,

6   Banyuls sur Mer, France.

7   Adriana Lopes dos Santos

8   Asian School of the Environment, Nanyang Technological University, 50 Nanyang Avenue,

9   Singapore

10   Centro de Genómica, Ecología y Medio Ambiente, Facultad de Ciencias, Universidad Mayor.

11   Camino La Pirámide 5750, Huechuraba. Santiago, Chile.

12   Wenche Eikrem

13   Norwegian Institute for Water Research, Gaustadallèen 21, 0349, Oslo, Norway.

14   University of Oslo, Department of Biosciences, P.O. box 1066 Blindern, 0316, Oslo, Norway.

15   Natural History Museum, University of Oslo, P.O. box 1172 Blindern, 0318 Oslo, Norway.

16   Catherine Gérikas Ribeiro and Priscillia Gourvil

17   Sorbonne Université, CNRS, UMR7144, Station Biologique de Roscoff, Roscoff, France.

18   Sergio Balzano

19   Stazione Zoologica Anton Dohrn, Istituto Nazionale di Biologia, Ecologia e Biotecnologie

20   Marine, Naples, Italy.

21

22   Marie-Line Escande and Hervé Moreau

1

23   Integrative Marine Biology Laboratory (BIOM), CNRS, UMR7232, Sorbonne Université,

24   Banyuls sur Mer, France.

25   Daniel Vaulot

26   Sorbonne Université, CNRS, UMR7144, Station Biologique de Roscoff, Roscoff, France.

27   Asian School of the Environment, Nanyang Technological University, 50 Nanyang Avenue,

28   Singapore.

29

30   [2]Corresponding author: Sheree Yau, sheeyau@gmail.com

31   [3]Present address: Department of Marine Biology and Oceanography, Institute of Marine Sciences

32   (ICM), CSIC, Barcelona, Spain.

33   Running Title: *Mantoniella* species from the high Arctic

34

Abstract

Members of the class Mamiellophyceae comprise species that can dominate picophytoplankton diversity in polar waters. Yet polar species are often morphologically indistinguishable from temperate species, although clearly separated by molecular features. Here we examine four Mamiellophyceae strains from the Canadian Arctic. The 18S rRNA and Internal Transcribed Spacer 2 (ITS2) gene phylogeny place these strains within the family Mamiellaceae (Mamiellales, Mamiellophyceae) in two separate clades of the genus *Mantoniella*. ITS2 synapomorphies support their placement as two new species, *Mantoniella beaufortii* and *Mantoniella baffinensis*. Both species have round green cells with diameter between 3–5 µm, one long flagellum and a short flagellum (~1 µm) and are covered by spiderweb-like scales, making both species similar to other *Mantoniella* species. Morphologically, *M. beaufortii* and *M. baffinensis* are most similar to the cosmopolitan *M. squamata* with only minor differences in scale structure distinguishing them. Screening of global marine metabarcoding datasets indicates *M. beaufortii* has only been recorded in seawater and sea ice samples from the Arctic while no environmental barcode matches *M. baffinensis*. Like other Mamiellophyceae genera that have distinct polar and temperate species, the polar distribution of these new species suggests they are cold or ice-adapted *Mantoniella* species.

Key index words: Arctic; ITS; Mamiellophyceae; *Mantoniella*; metabarcoding; picophytoplankton; polar

Abbreviations: rRNA, ribosomal RNA; ITS2, internal transcribed spacer 2; compensatory base change, CBC; hemi-CBC, hCBC; TEM, transmission electron microscopy

Introduction

Over the last decades the taxonomy of the green algae has gone through a profound reorganization. The class Prasinophyceae, initially defined as scaly flagellates (Moestrup and Throndsen 1988), has been rearranged into several new classes such as the Chlorodendrophyceae, Chloropicophyceae and Mamiellophyceae (Massjuk 2006, Marin and Melkonian 2010, Lopes dos Santos et al. 2017b) as well as clades without formal names (Guillou et al. 2004, Tragin et al. 2016) leading to the class name Prasinophyceae to be abandoned. The Mamiellophyceae are ecologically successful and particularly dominant in marine coastal waters (Lopes dos Santos et al. 2017a, Tragin and Vaulot 2018). The first scaled species of Mamiellophyceae observed were *Mantoniella squamata* (as *Micromonas squamata*, Manton and Parke 1960) and *Mamiella gilva* (as *Nephroselmis gilva*, Parke and Rayns 1964). Moestrup (1984) erected the family Mamiellaceae, which included *Mantoniella* and *Mamiella,* with *Mamiella gilva* designated as the type species. Mamiellophyceae comprises three orders: Monomastigales, with one freshwater genus *Monomastix*; Dolichomastigales, with two genera *Crustomastix* and *Dolichomastix*; Mamiellales, which currently comprises five genera *Bathycoccus*, *Mamiella*, *Mantoniella*, *Micromonas* and *Ostreococcus.* As these genera are morphologically heterogeneous, with *Micromonas* and *Ostreococcus* lacking scales and *Bathycoccus* and *Ostreococcus* lacking flagella, the monophyly of Mamiellophyceae was established based on nuclear and plastid rRNA sequence and secondary structure analyses (Marin and Melkonian 2010).

Molecular analyses of the Mamiellophyceae have permitted the description of otherwise morphologically indistinguishable cryptic species. For example, wide genetic diversity has been shown to exist between morphologically identical *Ostreococcus* species where less than 1%

4

80   difference in the 18S rRNA gene corresponds to up to 30% of variation in orthologous protein

81   coding sequences (Palenik et al. 2007, Piganeau et al. 2011). From an early stage, 18S rRNA-

82   defined clades of *Micromonas* and *Ostreococcus* were observed to have distinct geographic

83   distributions, suggesting their genetic variation reflected adaptations to ecological niches

84   (Rodríguez et al. 2005, Foulon et al. 2008) and that these clades represented distinct species.

85   *Ostreococcus* is divided into rare species restricted to estuarine (*O. mediterraneus*) and coastal

86   environments (*O. tauri*), as well as more abundant oceanic species (*O. lucimarinus* and clade B)

87   (Demir-Hilton et al. 2011, Treusch et al. 2012, Hu et al. 2016, Simmons et al. 2016).

88   *Micromonas* cells were observed to be abundant in the Arctic Ocean (Throndsen and Kristiansen

89   1991, Sherr et al. 2003, Not et al. 2005) that subsequent 18S rRNA analyses revealed them to

90   belong to a clade with an Arctic distribution (Lovejoy et al. 2007, Balzano et al. 2012).

91   *Micromonas* has since been revised defining the Arctic clade as the species *M. polaris*, and

92   species originating from lower latitudes as *M. bravo*, *M. commoda* and *M. pusilla* (Simon et al.

93   2017). Similarly, in *Mantoniella*, *M. antarctica* was described from the Antarctic whereas

94   *M. squamata* was cosmopolitan (Marchant et al. 1989).

95   Three picophytoplanktonic strains (RCC2285, RCC2288 and RCC2497) were isolated in the

96   Canadian Arctic from mesophilic surface water sampled at two sites in the Beaufort Sea in the

97   summer of 2009 as part of the MALINA cruise (Balzano et al. 2012). A fourth strain (RCC5418)

98   was subsequently isolated from sea ice collected in Baffin Bay in the spring as part of the Green

99   Edge project. We performed a combination of molecular, morphological and pigment

100   characterization of these isolates, which we propose to constitute two novel *Mantoniella* species,

101   *M. beaufortii* and *M. baffinensis*, restricted to polar environments.

Methods

Culture conditions. Strains RCC2285, RCC2288, and RCC2497 were isolated from seawater

collected at two sites (70°30'N, 135°30'W and 70°34'N, 145°24W) in the Beaufort Sea in the

summer of 2009 as part of the MALINA cruise as described previously (Balzano et al. 2012).

Strain RCC5418 was isolated from the Green Edge project Ice Camp

(http://www.greenedgeproject.info/), a sampling site on the sea ice near the village of

Qikiqtarjuaq (67°28.784N, 63°47.372W). Sampling was conducted between 20 April and 27

July, 2016, beginning in completely snow covered conditions followed by bare ice and ending

when the ice was broken out. Sea ice from 23 May 2016 was melted overnight and 200 mL was

gravity filtered (Sartorius filtration system) through 3 µm pore size polycarbonate filters

(Millipore Isopore membrane, 47 mm). 500 µL of filtrate was enriched by addition to 15 mL of

L1 medium (NCMA, Bigelow Laboratory for Ocean Sciences, USA). The enrichment culture

was purified by dilution to 10 cells per well in a 96 deep-well plate (Eppendorf) and incubated

under white light (100 µE m^{-2} s^{-1}) in a 12:12 h light: dark cycle at 4°C. Cell growth was observed

by the development of coloration after a few weeks. Culture purity was assessed by flow

cytometry (Becton Dickinson, Accuri C6). After confirmation of the purity, the culture was

transferred in a 50 mL ventilated flask (Sarstedt). Cultures are maintained in the Roscoff Culture

Collection (http://roscoff-culture-collection.org/) in K/2 (Keller et al. 1987) or L1 medium at

4ºC under a 12:12 h light: dark cycle at 100 µE light intensity. RCC2285 has been lost from

culture since molecular analyses (described below) were performed. For pigment analysis and

electron microscopy, RCC2288 was grown at 7ºC under continuous light at 100 µE intensity in

L1 medium prepared using autoclaved seawater from offshore Mediterranean Sea water diluted

10% with MilliQ water and filtered prior to use through 0.22 µm filters. Holotype specimens

125 were deposited in O (Natural History Museum, University of Oslo), herbarium acronym follows

126 Thiers (2019).

127

128 *Sequences.* Nuclear 18S rRNA and the Internal Transcribed Spacers (ITS) 1 and 2, as well as the

129 5.8S rRNA gene were retrieved from GenBank for strains RCC2288, RCC2497 and RCC2285

130 (Balzano et al. 2012). For RCC5418 and RCC5150 (*M. antarctica*), cells were harvested in

131 exponential growth phase and concentrated by centrifugation. Total nucleic acids were extracted

132 using the Nucleospin Plant II kit (Macherey-Nagel, Düren, DE) following the manufacturer's

133 instructions. The nearly full length nuclear 18S rRNA gene (only RCC5418) and the region

134 containing the Internal Transcribed Spacers (ITS) 1 and 2, as well as the 5.8S rRNA gene were

135 obtained by PCR amplification using universal primers (Supplementary Table 1). PCR products

136 were directly sequenced at the Macrogen Company (Korea) and sequences have been deposited

137 to Genbank under accession numbers MH516003, MH516002 and MH542162.

138

139 *ITS2 secondary structure*. The ITS2 secondary structure from the strains listed in Table 1 was

140 predicted using the Mfold web interface (Zuker 2003) under the default options with the folding

141 temperature fixed at 37ºC, resulting in multiple alternative folding patterns per sequence. The

142 preliminary structure for each sequence was chosen based on similarities found among the other

143 structures proposed for Mamiellophyceae (Marin and Melkonian 2010, Simon et al. 2017) as

144 well as on the presence of previously defined ITS2 hallmarks defined by Coleman (Mai and

145 Coleman 1997, Coleman 2000, 2003, 2007). Exported secondary structures in Vienna format and

146 the respective nucleotide sequences were aligned, visualized using 4SALE version 1.7 (Seibel et

147 al. 2008) and manually edited through extensive comparative analysis of each position

148 (nucleotide) in sequences from representatives of the Mamiellophyceae. The ITS2

149 synapomorphy analysis was confined to those positions that formed conserved base pairs in all

150 members of the Mamiellaceae order and the resulting intramolecular folding pattern (secondary

151 structure) of *Mantoniella* was drawn using CorelDRAW X7. A Vienna file containing the ITS2

152 sequences and secondary structure is available at

153 https://doi.org/10.6084/m9.figshare.7472153.v1.

154

155 *Phylogenetic analyses*. Nuclear 18S rRNA sequences belonging to members of

156 Mamiellophyceae were retrieved from GenBank (http://www.ncbi.nlm.nih.gov/). Two

157 environmental sequences (similar to strain sequences) were included in addition to the sequences

158 obtained from the cultures. Sequences were also obtained for the ITS2 region located between

159 the 5S and 23S rRNA genes. However, no environmental sequences were available to be

160 included in the 18S/ITS phylogenetic analyses.

161   Twenty-seven nuclear 18S rRNA and fourteen ITS2 sequences were aligned with MAFFT

162 using the E-INS-i and G-INS-i algorithms respectively (Katoh and Toh 2008). Alignments were

163 visualized and manually edited using Geneious 10.2.5 (Kearse et al. 2012). The ITS2 alignment

164 was further edited on the basis of conserved secondary structures (see above). The nuclear 18S

165 rRNA and ITS2 sequences from the Mamiellaceae members were concatenated using Geneious

166 10.2.5 (Kearse et al. 2012). Lengths of the resulting alignments were 1567 bp for 18S rRNA

167 (1242 identical sites, 295 variable and 191 parsimony-informative sites) and 1875 bp for

168 concatenated 18S-ITS sequences (1544 identical sites, 302 variable and 179 parsimony-

169 informative).

170   Phylogenetic reconstructions with two different methods, maximum likelihood (ML) and

171   Bayesian analyses, were performed using the nuclear Mamiellophyceae 18S rRNA and

172   Mamiellaceae concatenated 18S/ITS2 alignments.

173   The K2 + G + I model was selected for both sequence datasets based on the substitution

174   model selected through the Akaike information criterion (AIC) and the Bayesian information

175   criterion (BIC) options implemented in MEGA 6.06 (Tamura et al. 2013). ML analysis was

176   performed using PhyML 3.0 (Guindon et al. 2010) with SPR (Subtree Pruning and Regrafting)

177   tree topology search operations and approximate likelihood ratio test with Shimodaira-

178   Hasegawa-like procedure. Markov chain Monte Carlo iterations were conducted for 1,000,000

179   generations sampling every 100 generations with burning length 100,000 using MrBayes 3.2.2

180   (Ronquist and Huelsenbeck 2003) as implemented in Geneious (Kearse et al. 2012). Nodes were

181   considered as well supported when SH-like support values and Bayesian posterior probabilities

182   were higher than 0.8 and 0.95 respectively. The same criteria were used to represent the

183   sequences on the phylogenetic trees. Alignments are available at

184   https://doi.org/10.6084/m9.figshare.7472153.v1.

185   *Screening of environmental 18S rRNA sequencing datasets*. High-throughput sequencing

186   metabarcodes (V4 and V9 hypervariable regions) were obtained from several published polar

187   studies, as well as from the global sampling efforts Tara Oceans and Ocean Sampling Day

188   (OSD) (see Supplementary Table 2 for the full details and references for each project). We

189   screened these data as well as GenBank by BLASTn (98% identity cut-off) using RCC2288 18S

190   rRNA gene sequence as the search query. We aligned the retrieved environmental sequences and

191   metabarcodes with that of RCC2285, RCC2288, RCC2497, and RCC5418 using MAFFT as

192   implemented in Geneious version 10.0.7 (Kearse et al. 2012). This allowed the determination of

193   sequence signatures diagnostic of this species for both V4 and V9 (Supplementary Figures 1 and

194   2). The oceanic distribution of stations where cultures, clones and metabarcodes having these

195   signatures, as well as the stations from the metabarcoding surveys where no matching

196   metabarcodes have been found, were plotted with the R libraries ggplot2 and rworldmap. The R

197   script is available at https://vaulot.github.io/papers/RCC2288.html.

198

199   *Light microscopy*. Cells were observed using an Olympus BX51 microscope (Olympus,

200   Hamburg, Germany) with a 100× objective using differential interference contrast (DIC) and

201   imaged with a SPOT RT-slider digital camera (Diagnostics Instruments, Sterling Heights, MI,

202   USA).

203   For video-microscopy, cultures from RCC2288 and RCC2497 were observed with an inverted

204   Olympus IX70 inverted microscope using an x40 objective and equipped with an Infinity X

205   camera (https://www.lumenera.com/products/microscopy/infinityx-32.html). Short sequences

206   were recorded and edited with the Video de Luxe software (http://www.magix.com/fr/video-

207   deluxe/). Films were uploaded to Youtube (https://www.youtube.com/channel/UCsYoz-

208   aSJlJesyDNj6ZVolQ/videos). Video microscopy of swimming behavior of RCC2288

209   (https://youtu.be/CGKNxzfGUvQ), RCC2497 (https://youtu.be/rRNuk5Lx7Aw), and RCC5418

210   (https://youtu.be/xoxCEl1cv4Q). The recording protocol is available at

211   dx.doi.org/10.17504/protocols.io.k24cygw.

212

213   *Transmission Electron Microscopy*. Positive-stained whole mount cells were prepared as

214   described by Moestrup (1984), where cultures were directly deposited on formvar coated copper

215   grids and stained with 2% uranyl acetate. TEM thin-sections was performed as previously

216 described (Derelle et al. 2008). Briefly, fixed RCC2288 cells (1% glutaraldehyde) from an

217 exponentially growing culture were suspended in molten (37°C) 1% low melting point agarose.

218 The agarose cell plug was fixed, washed, dehydrated in ethanol and embedded in Epon 812.

219 Ultra-thin sections (80–90 nm) were placed on a 300 mesh copper grid and stained with uranyl

220 acetate for 15 min, followed by lead citrate staining for 2 min. The cells were visualized with

221 Hitachi H 7500 and H-9500 transmission electron microscopes.

222

223 *Pigment analysis*. Pigments were extracted from RCC2288 cells in late exponential phase as

224 previously described (Ras et al. 2008). Briefly, cells were collected on 0.7 μm particle retention

225 size filters (GF/F Whatman), pigments extracted for 2 hours in 100% methanol, then subjected to

226 ultrasonic disruption and clarified by filtration through 0.2 μm pore-size filters (PTFE). Pigments

227 were detected using high performance liquid chromatography (HPLC, Agilent Technologies

228 1200) over the 24 h after the extraction.

229 # Results and Discussion

230 *Taxonomy section. Mantoniella beaufortii* Yau, Lopes dos Santos and Eikrem sp. nov.

231 Description: Cells round measuring 3.7 ± 0.4 μm in diameter with one long (16.3 ± 2.6 μm)

232 and one short flagellum (~1 μm). Cell body and flagella covered in imbricated spiderweb scales.

233 Flagellar hair scales present composed of two parallel rows of subunits. Long flagellum tip has

234 tuft of three hair scales. Scales produced in Golgi body. Golgi body located beneath and to one

235 side of basal bodies. One green chloroplast with pyrenoid surrounded by starch and a stigma

236 composed of a single layer of oil droplets (~0.1 μm). Ejectosomes composed of fibrils located at

237 periphery of cell. Cell bodies with sub-quadrangular to oval scales (~0.2 μm). Body scales

11

238   heptaradial, with seven major spokes radiating from center, number of spokes increasing towards

239   the periphery. Six or more concentric ribs divide the scale into segments. Flagella with

240   hexaradial oval scales composed of six spokes increasing in number towards the periphery. Six

241   or more concentric ribs divide the scale into segments. Combined nucleotide sequences of the

242   18S rRNA (JN934679) and ITS2 rRNA (JQ413369) are species specific.

243   Holotype: Accession number O-A10010, plastic embedded specimen, 14 July 2009, from

244   surface water, MALINA cruise leg 1b. Figure 4 shows cells from the embedding. Culture

245   deposited in The Roscoff Culture Collection as RCC2288.

246   Type locality: Beaufort Sea in the Arctic Ocean (70°30'N, 135°30'W).

247   Etymology: Named for its geographical provenance.

248

249   *Mantoniella baffinensis* Yau, Lopes dos Santos and Eikrem sp. nov.

250   Description: Cells measuring 4.7 ± 0.5 μm with one long flagellum of 21.8 ± 5.1 μm and one

251   short flagellum (~1 μm). Cell body and flagella covered in imbricated spiderweb scales. Flagellar

252   hair scales present composed of two parallel rows of subunits. Long flagellum tip has tuft of

253   three hair scales. Cell bodies with sub-quadrangular to oval scales (~0.2 μm). Body scales

254   octaradial with eight major radial spokes radiating from center, number of spokes increasing

255   towards the periphery. Seven or more concentric ribs divide the scale into segments. Flagella

256   with heptaradial, oval scales composed of seven spokes increasing in number towards the

257   periphery. Six or more concentric ribs divide the scale into segments. Combined nucleotide

258   sequences of the nuclear 18S rRNA (MH516003) and ITS2 rRNA (MH542162) are species

259   specific.

260   Holotype: Accession number O-A10011, plastic embedded specimen, 23 May 2016, from

261   surface sea ice, Green Edge project Ice Camp. Culture deposited in The Roscoff Culture

262   Collection as RCC5418.

263   Type locality: Surface sea ice off the coast of Baffin Island in Baffin Bay (67°28'N, 63°46'W).

264   Etymology: Named for its geographical provenance.

265

266   *Phylogeny and ITS signatures.* The phylogenetic tree based on nearly full-length nuclear 18S

267   rRNA sequences obtained from the novel polar strains RCC2288, RCC2285, RCC2497 and

268   RCC5418 (Table 1), and environmental sequences retrieved from GenBank indicated that these

269   strains belong to the family Mamiellaceae (Supplementary Figure 3). The analysis also recovered

270   the major genera within Mamiellales: *Bathycoccus*, *Ostreococcus*, *Micromonas*, *Mantoniella* and

271   *Mamiella* (Marin and Melkonian 2010). Dolichomastigales and Monomastigales were the basal

272   orders in Mamiellophyceae with *Monomastix opisthostigma* type species used as an outgroup.

273   Strains RCC2485, RCC2288 and RCC2497 isolated during the MALINA cruise in the Beaufort

274   Sea and strain RCC5418 isolated from Baffin Bay during the Green Edge project Ice Camp

275   formed a well-supported clade together with two environmental sequences (clone MALINA

276   St320 3m Nano ES069 D8 and clone 4-E5), which also originated from Arctic Ocean samples.

277   The two described *Mantoniella* species (*M. squamata* and *M. antarctica*) were not monophyletic

278   in our analysis using the nuclear 18S rRNA, as reported by Marin and Melkonian (2010)

279   (Supplementary Figure 3).

280   In contrast, the phylogenetic tree based on concatenated 18S/ITS2 alignments suggested that

281   our strains belong in *Mantoniella* (Figure 1). The grouping of our strains within *Mantionella* in

282   the concatenated 18S/ITS tree was consistent with a recent nuclear multigene phylogeny based

13

283   on 127 concatenated genes from related Chlorophyta species that also included RCC2288 with

284   *Mantoniella* species (Lopes dos Santos et al. 2017b). This indicated the 18S/ITS2 tree reflects

285   the evolutionary history of the nuclear genome supporting the position of *Mantoniella* and our

286   strains diverging from the same common ancestor.

287   The average distance between strains RCC2485, RCC2288 and RCC2497 was low (0.5% of

288   segregating sites over the near full-length 18S rRNA gene), suggesting that these strains

289   corresponded to a single species that we named *Mantoniella beaufortii* (see Taxonomy section).

290   In contrast, the well-supported placement of strain RCC5418 on an earlier diverging branch

291   within the *Mantoniella* clade, as well as the 1% average distance between RCC5418 and the

292   other strains, suggested it represents another species, named here *Mantoniella baffinensis*.

293   To substantiate the description of *M. beaufortii* and *M. baffinensis* as new species, we

294   investigated ITS2 synapomorphies of the different *Mantoniella* species. Although the use of

295   ITS2 in taxonomy should be considered with caution (Müller et al. 2007, Caisová et al. 2011),

296   several studies have shown the power of using ITS2 sequences in delimiting biological species,

297   especially in microalgal studies (e.g. Coleman 2007, Caisová et al. 2011) including green algae

298   (Subirana et al. 2013, Simon et al. 2017). For example, ITS sequencing contributed to

299   distinguishing the Arctic diatom *Chaetoceros neogracilis* from an Antarctic *Chaetoceros* sp. that

300   shared nearly identical 18S rRNA genes (Balzano et al. 2017). The analysis of ITS2 secondary

301   structure in addition to molecular signatures of nuclear and plastid SSU rRNA genes supported

302   the description of Chloropicophyceae clades as distinct species, despite the absence of clear

303   morphological differences (Lopes dos Santos et al. 2017b). This conclusion has been further

304   supported by recent phylogenetic analyses of chloroplast and mitochondrial genomes (Turmel et

305   al. 2019). The computed ITS2 secondary structure of the new *Mantoniella* strains contained the

306 four helix domains found in many eukaryotic taxa (Supplementary Figure 4), in addition to Helix

307 B9. The intramolecular folding pattern of the ITS2 transcript from *M. beaufortii* and

308 *M. baffinensis* was very similar to the one from *M. squamata* and *M. antarctica* (Supplementary

309 Figure 4). The universal hallmarks proposed by Mai and Coleman et al. (1997) and Schultz et al.

310 (2005) were present in Helices II and III of the Mamiellaceae. These were the Y-Y (pyrimidine-

311 pyrimidine) mismatch at conserved base pair 7 in Helix II (Figure 2) and YRRY (pyrimidine-

312 purine-pyrimidine) motif at conserved positions 28–31 on the 5' side of Helix III

313 (Supplementary Figure 5A). In all four strains, the Y-Y mismatch was represented by the pair U-

314 U and the YRRY motif by the sequence UGGU.

315   The structural comparison at each base pair position within the ITS2 helices identified several

316 compensatory base changes (CBCs) and single-side changes or hemi-CBCs (hCBCs), as well as

317 conserved base pair positions among *Mantoniella* species (Supplementary Figure 4). Note that

318 we only considered hCBCs at positions where the nucleotide bond was preserved. No CBCs

319 were found between the three *M. beaufortii* strains consistent with their designation as a single

320 species. However, three hCBCs were detected in Helix II at positions 15 and 17 (Figure 2) and

321 Helix III at position 12 (Supplementary Figure 5A). Three CBCs were detected in Helices I

322 (position 4), II (position 15) and IV (position 22) between *M. beaufortii* and *M. baffinensis*,

323 supporting the separation of these strains into two distinct species (Figure 2 and Supplementary

324 Figure 4). When possible, the evolutionary steps of the identified CBCs and hCBCs were

325 mapped upon branches of the Mamiellaceae phylogenetic tree that was constructed based on the

326 concatenated 18S/ITS2 (Figure 2 and Supplementary Figure 4) to distinguish synapomorphies

327 from homoplasious changes (e.g. parallelisms and reversals). Few hypervariable positions

328 showing several changes (CBCs and hCBCs) could not be unambiguously mapped upon the tree.

329

Morphology and ultrastructure. Under light microscopy, the cells of the new strains were green

and round with one long and one short reduced flagellum (~1 μm), which were inserted almost

perpendicularly to the cell (Figure 3). They swam with their flagella directed posteriorly, pushing

the cell. Occasionally the cells ceased movement, pirouetted and took off again in a different

direction (video links in the Materials and Methods). All strains possessed a stigma, visible in

light microscopy as a red eyespot located opposite the flagella. Although there are no

morphological characters that are unique to the mamiellophyceans and shared by all of its

members, the new strains closely resembled *Mantoniella* and *Mamiella*, which are similarly

small round bi-flagellated cells (see Supplementary Table 3 for morphological characters in

described Mamiellophyceae). However, the flagella of *Mamiella* are of equal or near equal

lengths (Moestrup 1984), so clearly the unequal flagella observed in our strains conform with

described *Mantoniella* species, *M. squamata* and *M. antarctica* (Barlow and Cattolico 1980,

Marchant et al. 1989). The new strains were thus morphologically indistinguishable by light

microscopy from *Mantoniella* species, supporting their placement in the genus.

The new strains were in the size range (Table 2) reported for *M. squamata* (3–6.5 μm) and

M. antarctica (2.8–5 μm) (Manton and Parke 1960, Marchant et al. 1989). Nonetheless,

M. beaufortii strains were significantly smaller than *M. baffinensis* in cell diameter and average

long flagellum length (Table 2) providing a means to distinguish the two new *Mantoniella*

species from each other with light microscopy.

Transmission Electron Microscopy (TEM) of thin sections (Figure 4) and whole mounts

(Figure 5) of the new strains provided details of their internal and external morphological

features. The single chloroplast was cup-shaped with a pyrenoid surrounded by starch tubules

352   running through the pyrenoid. The stigma was composed of a single layer of oil droplets

353   (approximately 0.1 µm in diameter) (Figure 4A) and located at the periphery of the chloroplast

354   facing the cell membrane, conforming to the description of the family Mamiellaceae (Marin and

355   Melkonian 2010). Several large ejectosomes composed of fibrils were present at the cell

356   periphery (Figure 4D and E). They are common in the Mamiellales (Moestrup 1984, Marchant et

357   al. 1989) and are perhaps used to deter grazers.

358   One of the most salient features of the Mamiellophyceae is the presence of organic scales

359   covering the cell, the most common of which comprise radiating and concentric ribs resembling

360   spiderwebs that are present in the scale-bearing Mamiellales (*Bathycoccus*, *Mamiella* and

361   *Mantoniella*), as well as *Dolichomastix* (Supplementary Table 3). We examined the whole

362   mounts of the new *Mantoniella* species to establish the presence of scales and determine if they

363   were morphologically distinguishable from related species, as *M. antarctica* (Marchant et al.

364   1989) and *M. gilva* (Moestrup 1984) each have a unique type that differentiate them from other

365   Mamiellales.

366   The flagella and cell bodies of the new strains were covered in imbricated spiderweb-like

367   scales (Figure 5) measuring approximately 0.2 µm. The scales were produced in the Golgi body

368   (Figure 4B). The body scales were sub-quadrangular to oval whereas the flagellar scales were

369   oval (Figure 5). Spiderweb scales had 6–8 major spokes radiating from the center with the

370   number of spokes increasing towards the periphery and six or more concentric ribs dividing the

371   scale into segments. In addition, there were some small scales (approximately 0.1 µm) on the cell

372   body composed of four spokes (increasing to eight) and separated by four, more or less

373   concentric, ribs (Figure 5D, G). The flagella were also covered by lateral hair scales, which were

374   composed of two parallel rows of globular subunits. At the tip of the long flagellum there was a

375   tuft of three hair scales, for which the subunits were more closely packed together than the lateral

376   hair scales (Figure 5). The hair scales of the new strains were identical to the "*Tetraselmis*-type"

377   T-hairs previously described in *Mantoniella* and *Mamiella* (Marin and Melkonian 1994). This

378   structure is otherwise only seen in *Dolichomastix lepidota* and differs from the smooth tubular T-

379   hairs of *Dolichomastix tenuilepis* and *Crustomastix* (Marin and Melkonian 1994, Zingone et al.

380   2002)(Supplementary Table 3).

381   Comparison of the spiderweb scales between *Mantoniella* species (Table 3) showed the new

382   species differ significantly from *M. antarctica*, which possesses lace-like scales with six or seven

383   radial ribs with very few concentric ribs (Marchant et al. 1989). Morphologically, the spiderweb

384   scales of the new species most resembled *M. squamata*, which has large heptaradial flagellar

385   scales, octaradial body scales and a few additional small tetraradial body scales (Marchant et al.

386   1989). Indeed, the spiderweb scales of *M. baffinensis* (Figure 5) were structurally

387   indistinguishable from *M. squamata*. In contrast, *M. beaufortii* shared the small tetraradial body

388   scales but possessed hexaradial flagellar scales and heptaradial body scales, potentially allowing

389   it to be differentiated from the other *Mantoniella* based on the number of radial spokes of the

390   spiderweb scales.

391

392   *Pigment composition.* Pigment to chlorophyll *a* ratios of *M. beaufortii* RCC2288 were compared

393   to a selection of other Chlorophyta species (Figure 6, Supplementary Table 4) from previous

394   studies (Latasa et al. 2004, Lopes dos Santos et al. 2016), as pigments are useful phenotypic

395   traits. Chlorophyll *a* and *b*, characteristics of Chlorophyta, were detected, as well as the basic set

396   of carotenoids found in the prasinophytes: neoxanthin, violaxanthin, lutein, zeaxanthin,

397   antheraxanthin and β-carotene. The additional presence of prasinoxanthin, micromonal and

398   uriolide placed RCC2288 in the PRASINO-3B group of prasinophyte green algae, *sensu* Jeffrey

399   et al. (2011). This pigment-based grouping showed good agreement with the molecular

400   phylogeny of Mamiellales, where the presence of prasinoxanthin, micromonal and the

401   Unidentified M1 pigment are diagnostic of the order (Marin and Melkonian 2010). We did not

402   detect Unidentified M1 in RCC2288, but as our analysis method differed from previous work

403   (Latasa et al. 2004) and we relied on matching its chromatographic and spectral characteristics,

404   its absence requires further confirmation. Notwithstanding, the pigment complement of

405   RCC2288 was identical to other described Mamiellales (Figure 6, Supplementary Table 4),

406   coherent with its classification within this order.

407   As noted by Latasa et al. (2004), Mamiellales pigment profiles are remarkably comparable

408   (Figure 6), despite strains being cultured under very different conditions. Only a few carotenoids

409   differed substantially (at least two fold) in relative abundance between *M. beaufortii* and the two

410   other *M. squamata* strains analyzed: the concentration of neoxanthin, antheraxanthin and lutein

411   were higher, whereas that of Mg-DVP and uriolide were relatively lower (Figure 6,

412   Supplementary Table 4). Neoxanthin (associated with the light harvesting complex), as well as

413   antheraxanthin and lutein (both involved in photoprotection), have previously been shown to

414   increase significantly in *M. squamata* grown under continuous light compared to alternating

415   light/dark cycles (Böhme et al. 2002). Therefore, the relatively high ratio of these carotenoids

416   measured in *M. beaufortii* is consistent with growth under continuous light used with RCC2288.

417   Uriolide and Mg-DVP have been observed to increase with light intensity in *M. squamata*

418   (Böhme et al. 2002) and *Micromonas pusilla* (Laviale and Neveux 2011), respectively. Although

419   more physiological data are required to interpret their relative decrease in RCC2288, these

420   pigments are probably most responsive to light conditions (intensity and photoperiod).

421   Two unknown carotenoids were detected in RC2288, the first one having adsorption peaks at

422   412, 436 and 464 nm, and the second one at 452 nm (Supplementary Table 5). These were

423   relatively minor components comprising 2.7% and 1.5% of total carotenoids, respectively and

424   may represent carotenoids unique to *M. beaufortii*.

425

426   *Environmental distribution.* In order to obtain information on the distribution of these two new

427   species, we searched by BLAST both environmental GenBank sequences and published 18S V4

428   and V9 metabarcode data sets (Supplementary Table 2). This allowed the retrieval of a few 18S

429   rRNA sequences with higher than 98% similarity to the gene of RCC2288. Alignment of these

430   sequences with other Mamiellophyceae sequences revealed diagnostic positions in both the V4

431   and V9 hypervariable regions permitting *M. beaufortii* and *M. baffinensis* to be distinguished

432   from other Mamiellophyceae, especially other *Mamiella* and *Mantoniella* species

433   (Supplementary Figures 1 and 2). Signatures from the V4 region were clearer than from V9 due

434   to the fact that for some of the strains, the sequences did not extend to the end of the V9 region

435   (Supplementary Figure 2). In the V4 region, three signatures were observed, one common to

436   both species (A in Supplementary Figure 1), while the other two (B and C in Supplementary

437   Figure 1) differed between *M. beaufortii* and *baffinensis.*

438   No clone library or metabarcode sequences matched exactly *M. baffinensis*. In contrast, three

439   environmental sequences (KT814860, FN690725, JF698785) from clone libraries had signatures

440   similar to the *M. beaufortii* strains, two from Arctic Ocean water (Figure 7), including one

441   obtained during the MALINA cruise, and one from ice originating from the Gulf of Finland. V4

442   metabarcodes corresponding to *M. beaufortii* were found in the Ocean Sampling Day data set

443   (Kopf et al. 2015) that includes more than 150 coastal samples at a single station off East

444 Greenland as well as in three metabarcoding studies in the Arctic Ocean, one in the Beaufort Sea

445 performed during the MALINA cruise (Monier et al. 2015), one from Arctic sea ice (Stecher et

446 al. 2016) where it was found at three stations and one from the White Sea (Belevich et al. 2017),

447 also in the sea ice (Figure 7). No metabarcode corresponding to these two new species were

448 found in waters from either the Southern Ocean or off Antarctica (Figure 7 and Supplementary

449 Table 2). No metabarcodes from the V9 region corresponding to the two new species were found

450 in the Tara Oceans data set that covered mostly temperate and subtropical oceanic regions (de

451 Vargas et al. 2015). These data suggest that these species are restricted to polar Arctic regions

452 (although we cannot exclude that they may be found in the future in the Antarctic which has

453 been under-sampled until now) and are probably associated to sea ice although they can be

454 present in the sea water, and that *M. beaufortii* is more wide spread than *M. baffinensis*.

463   platform of the Oceanological Observatory of Banyuls and of the ABIMS bioinformatics

464   platform at the Roscoff Biological Station.

465

References

Balzano, S., Gourvil, P., Siano, R., Chanoine, M., Marie, D., Lessard, S., Sarno, D. & Vaulot, D. 2012. Diversity of cultured photosynthetic flagellates in the North East Pacific and Arctic Oceans in summer. *Biogeosciences* 9:4553–71.

Balzano, S., Percopo, I., Siano, R., Gourvil, P., Chanoine, M., Marie, D., Vaulot, D. & Sarno, D. 2017. Morphological and genetic diversity of Beaufort Sea diatoms with high contributions from the *Chaetoceros neogracilis* species complex. *J. Phycol.* 53:161–87.

Barlow, S. B. & Cattolico, R. A. 1980. Fine structure of the scale-covered green flagellate *Mantoniella squamata* (Manton et Parke) Desikachary. *Brit. Phycol. J.* 15:321–33.

Belevich, T. A., Ilyash, L. V., Milyutina, I. A., Logacheva, M. D., Goryunov, D. V. & Troitsky, A. V. 2017. Photosynthetic picoeukaryotes in the land-fast ice of the White Sea, Russia. *Microb. Ecol.* 1–16.

Böhme, K., Wilhelm, C. & Goss, R. 2002. Light regulation of carotenoid biosynthesis in the prasinophycean alga *Mantoniella squamata*. *Photochem. Photobiol. Sci.* 1:619–28.

Caisová, L., Marin, B. & Melkonian, M. 2011. A close-up view on ITS2 evolution and speciation - a case study in the Ulvophyceae (Chlorophyta, Viridiplantae). *BMC Evol. Biol.* 11:262.

Coleman, A. W. 2000. The significance of a coincidence between evolutionary landmarks found in mating affinity and a DNA sequence. *Protist* 151:1–9.

Coleman, A. W. 2003. ITS2 is a double-edged tool for eukaryote evolutionary comparisons. *Trends Genet.* 19:370–5.

Coleman, A. W. 2007. Pan-eukaryote ITS2 homologies revealed by RNA secondary structure. *Nucleic Acids Res.* 35:3322–9.

489   de Vargas, C., Audic, S., Henry, N., Decelle, J., Mahe, F., Logares, R., Lara, E., Berney, C., Le

490   Bescot, N., Probert, I., Carmichael, M., Poulain, J., Romac, S., Colin, S., Aury, J.-M.,

491   Bittner, L., Chaffron, S., Dunthorn, M., Engelen, S., Flegontova, O., Guidi, L., Horák, A.,

492   Jaillon, O., Lima-Mendez, G., Lukeš, J., Malviya, S., Morard, R., Mulot, M., Scalco, E.,

493   Siano, R., Vincent, F., Zingone, A., Dimier, C., Picheral, M., Searson, S., Kandels-Lewis,

494   S., *Tara* Oceans Coordinators, Acinas, S. G., Bork, P., Bowler, C., Gorsky, G., Grimsley,

495   N., Hingamp, P., Iudione, D., Not, F., Ogata, H., Pesant, S., Raes, J., Sieracki, M. E.,

496   Speich, S., Stemmann, L., Sunagawa, S., Weissenbach, J., Wincker, P. & Karsenti, E. 2015.

497   Eukaryotic plankton diversity in the sunlit ocean. *Science* 348:1261605.

498   Demir-Hilton, E., Sudek, S., Cuvelier, M. L., Gentemann, C. L., Zehr, J. P. & Worden, A. Z.

499   2011. Global distribution patterns of distinct clades of the photosynthetic picoeukaryote

500   *Ostreococcus*. *ISME J.* 5:1095–107.

501   Derelle, E., Ferraz, C., Escande, M.-L., Eychenié, S., Cooke, R., Piganeau, G., Desdevises, Y.

502   Bellec L., Moreau, H. & Grimsley, N. 2008. Life-cycle and genome of OtV5, a Large DNA

503   virus of the pelagic marine unicellular green alga *Ostreococcus tauri*. *PLoS One*. 3:e2250.

504   Foulon, E., Not, F., Jalabert, F., Cariou, T., Massana, R. & Simon, N. 2008. Ecological niche

505   partitioning in the picoplanktonic green alga *Micromonas pusilla*: Evidence from

506   environmental surveys using phylogenetic probes. *Environ. Microbiol.* 10:2433–43.

507   Guillou, L., Eikrem, W., Chrétiennot-Dinet, M.-J., Le Gall, F., Massana, R., Romari, K., Pedrós-

508   Alió, C. & Vaulot, D. 2004. Diversity of picoplanktonic prasinophytes assessed by direct

509   nuclear SSU rDNA sequencing of environmental samples and novel isolates retrieved from

510   oceanic and coastal marine ecosystems. *Protist* 155:193–214.

511   Guindon, S., Dufayard, J.-F., Lefort, V. & Anisimova, M. 2010. New algorithms and methods to

512   estimate maximum-likelihoods phylogenies: Assessing the performance of PhyML 3.0.

513   *Syst. Biol.* 59:307–21.

514   Hu, Y. O. O., Karlson, B., Charvet, S. & Andersson, A. F. 2016. Diversity of pico- to

515   mesoplankton along the 2000 km salinity gradient of the baltic sea. *Front. Microbiol.* 7:1–

516   17.

517   Jeffrey, S. W., Wright, S. W. & Zapata, M. 2011. Microalgal classes and their signature

518   pigments. *In* Roy, S., Llewellyn, C. A., Egeland, E. S. & Johnsen, G. [Eds.] *Phytoplankton*

519   *Pigments: Characterization, Chemotaxonomy and Applications in Oceanography.*

520   Cambridge Univ Press, Cambridge. 3–77 pp.

521   Katoh, K. & Toh, H. 2008. Recent developments in the MAFFT multiple sequence alignment

522   program. *Brief. Bioinform.* 9:286–98.

523   Kearse, M., Moir, R., Wilson, A., Stones-Havas, S., Cheung, M., Sturrock, S., Buxton, S.,

524   Cooper, A., Markowitz, S., Duran, C., Thierer, T., Ashton, B., Meintjes, P. & Drummond,

525   A. 2012. Geneious Basic: An integrated and extendable desktop software platform for the

526   organization and analysis of sequence data. *Bioinformatics* 28:1647–9.

527   Keller, M. D., Selvin, R. C., Claus, W. & Guillard, R. R. L. 1987. Media for the culture of

528   oceanic ultraphytoplankton. *J. Phycol.* 23:633–8.

529   Kopf, A., Bicak, M., Kottmann, R., Schnetzer, J., Kostadinov, I., Lehmann, K., Fernandez-

530   Guerra, A., Jeanthon, C., Rahav, E., Ullrich, M., Wichels, A., Gunnar, G., Polymenakou, P.,

531   Kotoulas, G., Siam, R., Abdallah, R. Z., Sonnenschein, E. C., Cariou, T., O'Gara, F.,

532   Jackson, S., Orlic, S., Steinke, M., Busch, J., Duarte, B., Caçador, I., Canning-Clode, J.,

533   Bobrova, O., Marteinsson, V., Reynisson, E., Loureiro, C. M., Luna, G. M., Quero, G. M.,

534   Löscher, C. R., Kremp, A., DeLorenzo, M. E., Øvreås, L., Tolman, J., LaRoche, J., Penna,

535   A., Frischer, M., Davis, T., Katherine, B., Meyer, C. P., Ramos, S., Magalhães, C., Jude-

536   Lemeilleur, F., Aguirre-Macedo, M. L., Wang, S., Poulton, N., Jones, S., Collin, R.,

537   Fuhrman, J. A., Conan, P., Alonso, C., Stambler, N., Goodwin, K., Yakimov, M. M., Baltar,

538   F., Bodrossy, L., Van De Kamp, J., Frampton, D. M. F., Ostrowski, M., Van Ruth, P.,

539   Malthouse, P., Claus, S., Deneudt, K., Mortelmans, J., Pitois, S., Wallom, D., Salter, I.,

540   Costa, R., Schroeder, D. C., Kandil, M. M., Amaral, V., Biancalana, F., Santana, R.,

541   Pedrotti, M. L., Yoshida, T., Ogata, H., Ingleton, T., Munnik, K., Rodriguez-Ezpeleta, N.,

542   Berteaux-Lecellier, V., Wecker, P., Cancio, I., Vaulot, D., Bienhold, C., Ghazal, H.,

543   Chaouni, B., Essayeh, S., Ettamimi, S., Zaid, E. H., Boukhatem, N., Bouali, A., Chahboune,

544   R., Barrijal, S., Timinouni, M., El Otmani, F., Bennani, M., Mea, M., Todorova, N.,

545   Karamfilov, V., ten Hoopen, P., Cochrane, G., L'Haridon, S., Bizsel, K. C, Vezzi, A.,

546   Lauro, F. M., Martin, P., Jensen, R. M., Hinks, J., Gebbels, S., Rosselli, R., De Pascale, F.,

547   Schiavon, R., dos Santos, A., Villar, E., Pesant, S., Cataletto, B., Malfatti, F., Edirisinghe,

548   R., Herrera Silveira, J. A., Barbier, M., Turk, V., Tinta, T., Fuller, W. J., Salihoglu, I.,

549   Serakinci, N., Ergoren, M. C., Bresnan, E., Iriberri, J., Nyhus, P. A. F., Bente, E., Karlsen,

550   H. E., Golyshin, P. N., Gasol, J. M., Moncheva, S., Dzhembekova, N., Johnson, Z.,

551   Sinigalliano, C. D., Gidley, M. L., Zingone, A., Danovaro, R., Tsiamis, G., Clark, M. S.,

552   Costa, A. C., El Bour, M., Martins, A. M., Collins, R. E., Ducluzeau, A.-L., Martinez, J.,

553   Costello, M. J.m Amaral-Zettler, L. A., Gilbert, J. A., Davies, N., Field, D. & Glöckner, O.

554   2015. The ocean sampling day consortium. *Gigascience* 4:27.

555 Latasa, M., Scharek, R., Le Gall, F. & Guillou, L. 2004. Pigment suites and taxonomic groups in

556   Prasinophyceae. *J. Phycol.* 40:1149–55.

557 Laviale, M. & Neveux, J. 2011. Relationships between pigment ratios and growth irradiance in

558   11 marine phytoplankton species. *Mar. Ecol. Prog. Ser.* 425:63–77.

559   Lopes dos Santos, A., Gourvil, P., Rodríguez, F., Garrido, J. L. & Vaulot, D. 2016.

560   Photosynthetic pigments of oceanic Chlorophyta belonging to Prasinophytes clade VII. *J.*

561   *Phycol.* 52:148–55.

562   Lopes dos Santos, A., Gourvil, P., Tragin, M., Noël, M. H., Decelle, J., Romac, S. & Vaulot, D.

563   2017a. Diversity and oceanic distribution of prasinophytes clade VII, the dominant group of

564   green algae in oceanic waters. *ISME J.* 11:512–28.

565   Lopes dos Santos, A., Pollina, T., Gourvil, P., Corre, E., Marie, D., Garrido, J. L., Rodríguez, F.,

566   Noël, M.-H., Vaulot, D. & Eikrem, W. 2017b. Chloropicophyceae, a new class of

567   picophytoplanktonic prasinophytes. *Sci. Rep.* 7:14019.

568   Lovejoy, C., Vincent, W. F., Bonilla, S., Roy, S., Martineau, M. J., Terrado, R., Potvin, M.,

569   Massana, R. & Pedrós-Alió, C. 2007. Distribution, phylogeny, and growth of cold-adapted

570   picoprasinophytes in Arctic seas. *J. Phycol.* 43:78–89.

571   Mai, J. C. & Coleman, A. W. 1997. The internal transcribed spacer 2 exhibits a common

572   secondary structure in green algae and flowering plants. *J. Mol. Evol.* 44:258–71.

573   Manton, I. & Parke, M. 1960. Further observations on small green flagellates with special

574   reference to possible relatives of *Chromulina pusilla* Butcher. *J. Mar. Biol. Assoc.* 39:275–

575   98.

576   Marchant, H. J., Buck, K. R., Garrison, D. L. & Thomsen, H. A. 1989. *Mantoniella* in Antarctic

577   waters including the description of *M. antarctica* sp. nov. (Prasinophyceae). *J. Phycol.*

578   25:167–74.

579   Marin, B. & Melkonian, M. 1994. Flagellar hairs in prasinophytes (Chlorophyta): Ultrastructure

580   and distribution on the flagellar surface. *J. Phycol.* 30:659–78.

581   Marin, B. & Melkonian, M. 2010. Molecular phylogeny and classification of the

582   Mamiellophyceae class. nov. (Chlorophyta) based on sequence comparisons of the nuclear-

583   and plastid-encoded rRNA operons. *Protist* 161:304–36.

584   Massjuk, N.P. 2006. Chlorodendrophyceae class. nov. (Chlorophyta, Viridiplantae) in the

585   Ukrainian flora: I. Phylogenetic relations and taxonomical status. *Ukr. Bot. J.* 63:601–14.

586   Moestrup, Ø. 1984. Further studies on *Nephroselmis* and its allies (Prasinophyceae). II. *Mamiella*

587   gen. nov., Mamiellaceae fam. nov., Mamiellales ord. nov. *Nord. J. Bot.* 4:109–21.

588   Moestrup, Ø. & Throndsen, J. 1988. Light and electron microscopical studies on

589   *Pseudoscourfieldia marina*, a primitive scaly green flagellate (Prasinophyceae) with

590   posterior flagella. *Can. J. Bot.* 66:1415–34.

591   Monier, A., Me Comte, J., Babin, M., Forest, A., Matsuoka, A. & Lovejoy, C. 2015.

592   Oceanographic structure drives the assembly processes of microbial eukaryotic

593   communities. *ISME J.* 9:990–1002.

594   Müller, T., Philippi, N., Dandekar, T., Schultz, J. & Wolf, M. 2007. Distinguishing species. *RNA*

595   13: 1469–72.

596   Not, F., Massana, R., Latasa, M., Marie, D., Colson, C., Eikrem, W., Pedrós-Alió, C., Vaulot, D.

597   & Simon, N. 2005. Late summer community composition and abundance of photosynthetic

598   picoeukaryotes in Norwegian and Barents Seas. *Limnol. Oceanogr.* 50:1677–86.

599   Palenik, B., Grimwood, J., Aerts, A., Rouzé, P., Salamov, A., Putnam, N., Dupont, C.,

600   Jorgensen, R., Derelle, E., Rombauts, S., Zhou, K., Otillar, R., Merchant, S. S., Podel, S.,

601   Gaasterland, T., Napoli, C., Gendler, K., Manuell, A., Tai, V., Vallon, O., Piganeau, G.,

602   Jancek, S., Heijde, M., Jabbari, K., Bowler, C., Lohr, M., Robbens, S., Werner, G.,

603   Dubchak, I., Pazour, G. J., Ren, Q., Paulsen, I., Delwiche, C., Schmutz, J., Rokhsar, D., Van

604   de Peer, Y., Moreau, H. & Grigoriev, I. V. 2007. The tiny eukaryote *Ostreococcus* provides

605   genomic insights into the paradox of plankton speciation. *P. Natl. Acad. Sci. U.S.A.*

606   104:7705–10.

607 Park, M. & Rayns, D. G. 1964. Studies on marine flagellates. VII. *Nephroselmis gilva* sp. nov.

608   and some allied forms. *J. Mar. Biol. Ass. U.K.* 44:209–17.

609 Piganeau, G., Eyre-Walker, A., Grimsley, N. & Moreau, H. 2011. How and why DNA barcodes

610   underestimate the diversity of microbial eukaryotes. *PLoS One*. 6:e16342.

611 Ras, J., Claustre, H. & Uitz, J. 2008. Spatial variability of phytoplankton pigment distributions in

612   the Subtropical South Pacific Ocean: comparison between *in situ* and predicted data.

613   *Biogeosciences* 5:353–69.

614 Rodríguez, F., Derelle, E., Guillou, L., Le Gall, F., Vaulot, D. & Moreau, H. 2005. Ecotype

615   diversity in the marine picoeukaryote *Ostreococcus* (Chlorophyta, Prasinophyceae).

616   *Environ. Microbiol.* 7:853–9.

617 Ronquist, F. & Huelsenbeck, J. P. 2003. MrBAYES 3: Bayesian phylogenetic inference under

618   mixed models. *Bioinformatics* 19:1572–4.

619 Schultz, J., Maisel, S., Gerlach, D., Müller, T. & Wolf, M. 2005. A common core of secondary

620   structure of the internal transcribed spacer 2 (ITS2) throughout the Eukaryota. *RNA* 11:361–

621   4.

622 Seibel, P., Müller, T., Dandekar, T. & Wolf, M. 2008. Synchronous visual analysis and editing of

623   RNA sequence and secondary structure alignments using 4SALE. *BMC Res. Notes*. 1:91.

624 Sherr, E.B., Sherr, B.F., Wheeler, P. A. & Thompson, K. 2003. Temporal and spatial variation in

625   stocks of autotrophic and heterotrophic microbes in the upper water column of the central

626   Arctic Ocean. *Deep Sea Research Part I: Oceanographic Research Papers* 50:557–71.

627 Simmons, M. P., Sudek, S., Monier, A., Limardo, A. J., Jimenez, V., Perle, C. R., Elrod, V. A.,

628   Pennington, J. T. & Worden, A. Z. 2016. Abundance and biogeography of picoprasinophyte

629   ecotypes and other phytoplankton in the eastern North Pacific Ocean. *Appl. Environ.*

630   *Microbiol.* 82:1693–705.

631 Simon, N., Foulon, E., Grulois, D., Six, C., Desdevises, Y., Latimier, M., Le Gall, F., Tragin, M.,

632   Houdan, A., Derelle, E., Jouenne, F., Marie, D., Le Panse, S., Vaulot, D. & Marin, B. 2017.

633   Revision of the genus *Micromonas* Manton et Parke (Chlorophyta, Mamiellophyceae), of

634   the type species *M. pusilla* (Butcher) Manton et Parke of the species *M. commoda* van

635   Baren, Bachy and Worden and description of two new species based on the genetic and

636   phenotypic characterization of cultured isolates. *Protist* 168:612–35.

637 Subirana, L., Péquin, B., Michely, S., Escande, M-L., Meilland, J., Derelle, E., Marin, B.,

638   Piganeau, G., Desdevises, Y., Moreau, H. & Grimsley, N. H. 2013. Morphology, genome

639   plasticity, and phylogeny in the genus *Ostreococcus* reveal a cryptic species,

640   *O. mediterraneus* sp. nov. (Mamiellales, Mamiellophyceae). *Protist* 164: 643–659.

641 Stecher, A., Neuhaus, S., Lange, B., Frickenhaus, S., Beszteri, B., Kroth, P.G. & Valentin, K.

642   2016. rRNA and rDNA based assessment of sea ice protist biodiversity from the central

643   Arctic Ocean. *Eur. J. Phycol.* 51:31–46.

644 Tamura, K., Stecher, G., Peterson, D., Filipski, A. & Kumar, S. 2013. MEGA6: Molecular

645   evolutionary genetics analysis version 6.0. *Mol. Biol. Evol.* 30:2725–9.

646 Thiers, B. Index Herbariorum: A global directory of public herbaria and associated staff. New

647   York Botanical Garden's Virtual Herbarium. Available at: http://sweetgum.nybg.org/ih (last

648   accessed 20 August 2019)

649 Throndsen, J. & Kristiansen, S. 1991. *Micromonas pusilla* (Prasinophyceae) as part of pico- and

650 nanoplankton communities of the Barents Sea. *Polar Res.* 10:201–7.

651 Tragin, M., Lopes dos Santos, A., Christen, R. & Vaulot, D. 2016. Diversity and ecology of

652 green microalgae in marine systems: An overview based on 18S rRNA gene sequences.

653 *Perspect. Phycol.* 3:141–54.

654 Tragin, M. & Vaulot, D. 2018. Green microalgae in marine coastal waters: The Ocean Sampling

655 Day (OSD) dataset. *Sci. Rep.* 8:1–12.

656 Treusch, A. H., Demir-Hilton, E., Vergin, K. L., Worden, A. Z., Carlson, C. A, Donatz, M. G.,

657 Burton, R. M. & Giovannoni, S. J. 2012. Phytoplankton distribution patterns in the

658 northwestern Sargasso Sea revealed by small subunit rRNA genes from plastids. *ISME J.*

659 6:481–92.

660 Turmel, M., Lopes dos Santos, A., Otis, C., Sergerie, R. & Lemieux, C. 2019. Tracing the

661 evolution of the plastome and mitogenome in the Chloropicophyceae uncovered convergent

662 tRNA gene losses and a variant plastid genetic code. *Genome Biol. Evol.* 11: 1275–92.

663 Zingone, A., Borra, M., Brunet, C., Forlani, G., Kooistra, W. H. C. F. & Procaccini, G. 2002.

664 Phylogenetic position of *Crustomastix stigmatica* sp. nov. and *Dolichomastix tenuilepsis* in

665 relation to the Mamiellales (Prasinophyceae, Chlorophyta). *J. Phycol.* 38:1024–39.

666 Zuker, M. 2003. Mfold web server for nucleic acid folding and hybridization prediction. *Nucleic*

667 *Acids Res.* 31:3406–15.

668

669

670

671

672

Figures


674
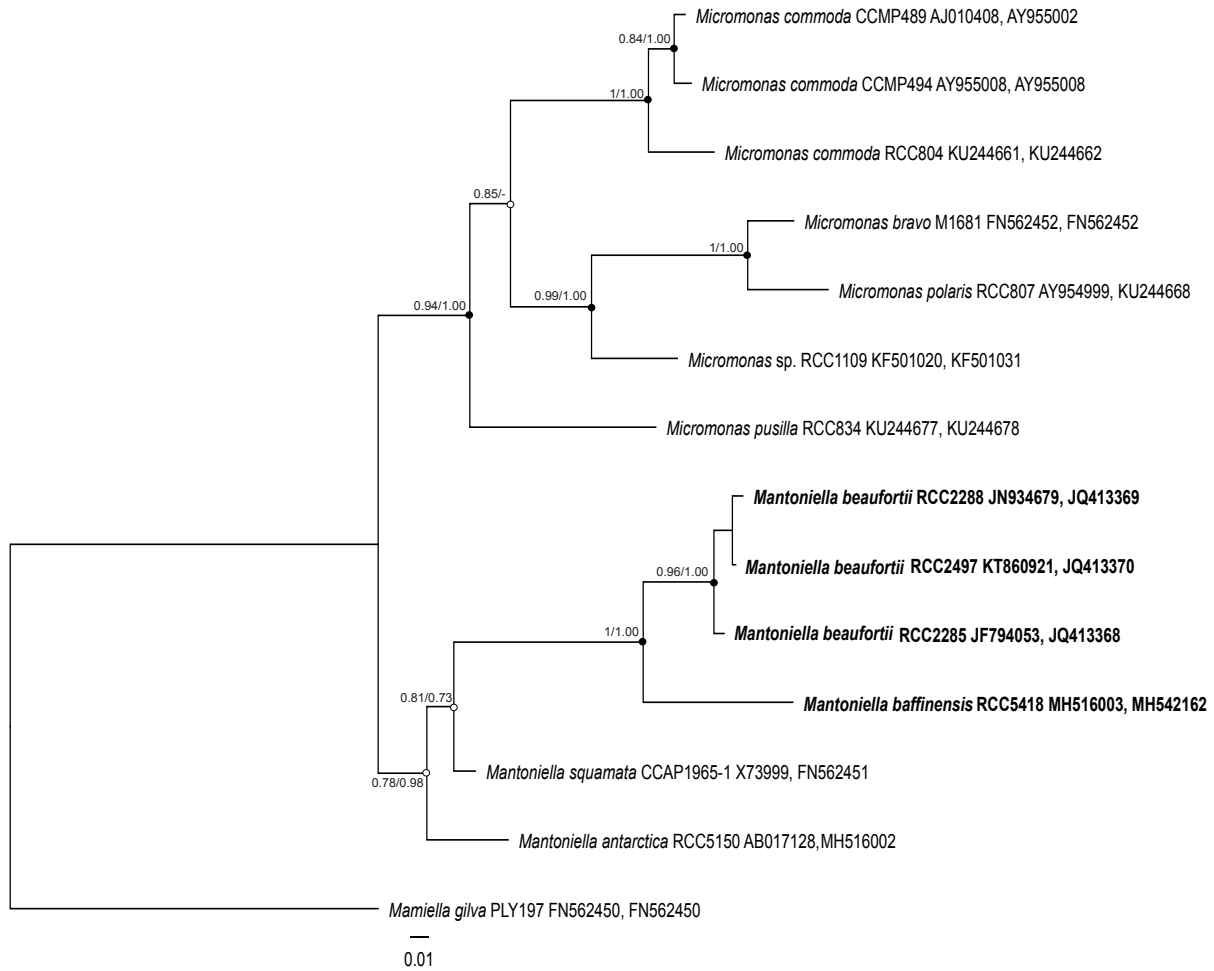
Figure 1. Maximum-likelihood tree inferred from concatenated 18S/ITS2 sequences of

Mamiellaceae. Solid dots correspond to nodes with significant support (> 0.8) for ML analysis

and Bayesian analysis (> 0.95). Empty dots correspond to nodes with non-significant support for

either ML or Bayesian analysis, or both.
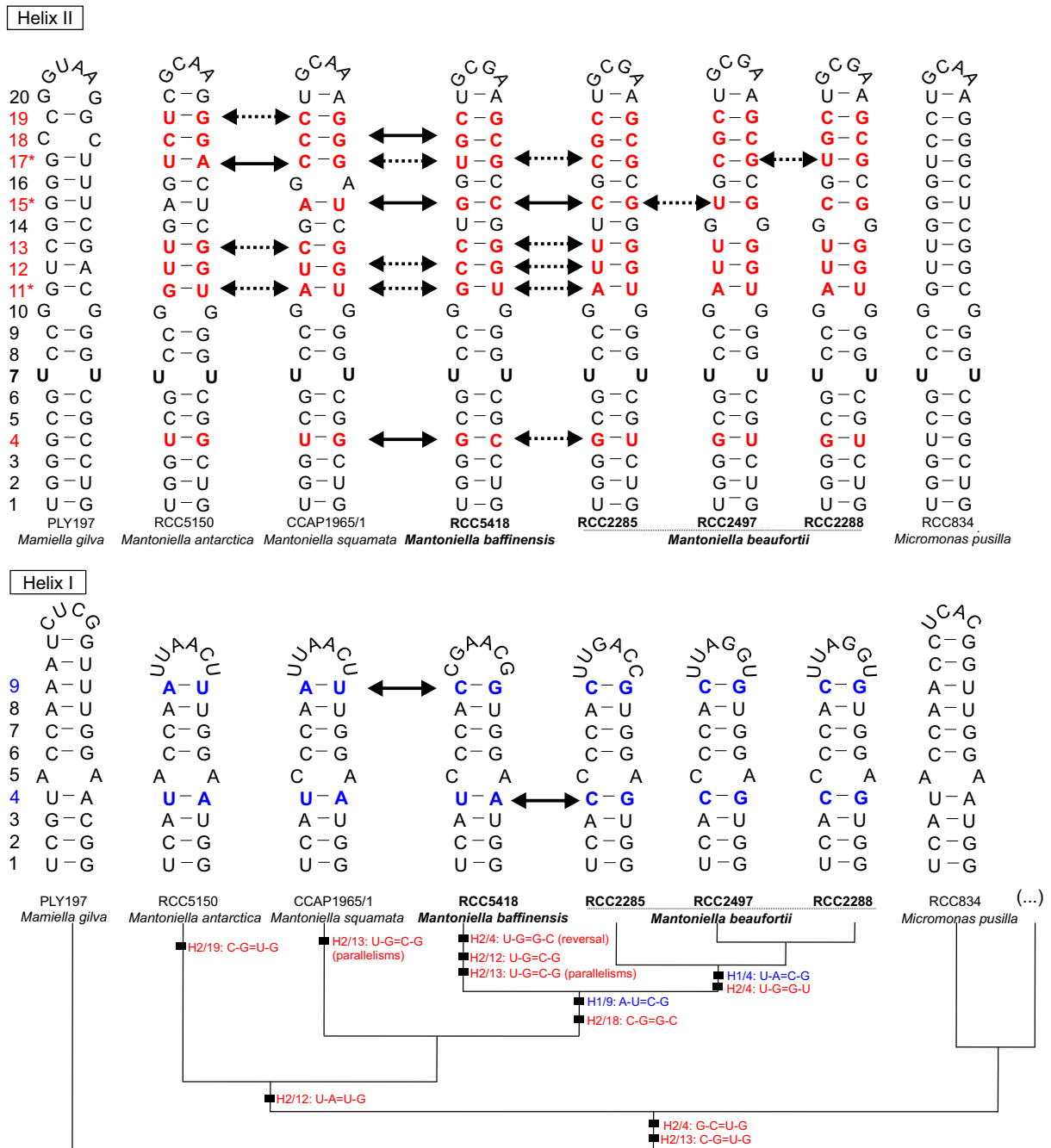
Figure 2. Molecular signatures of *Mantoniella* species based on comparison of ITS2 secondary structures within Mamiellaceae. Signatures in Helix I are shown in blue and Helix II in red. The conserved base pairs among the different groups are numbered. Compensatory base changes (CBCs) and hemi-CBCs (hCBSs) are highlighted by solid and dotted arrows respectively.

684   Hypervariable positions are marked by an asterisk (*). Ellipsis (…) represent the other clades

685   and species of *Micromonas*. The pyrimidine-pyrimidine (Y-Y) mismatch in Helix II is shown in

686   bold black. Single nucleotide substitutions are shown by grey nucleotides. Identified

687   homoplasious changes are shown as parallelisms and reversals.
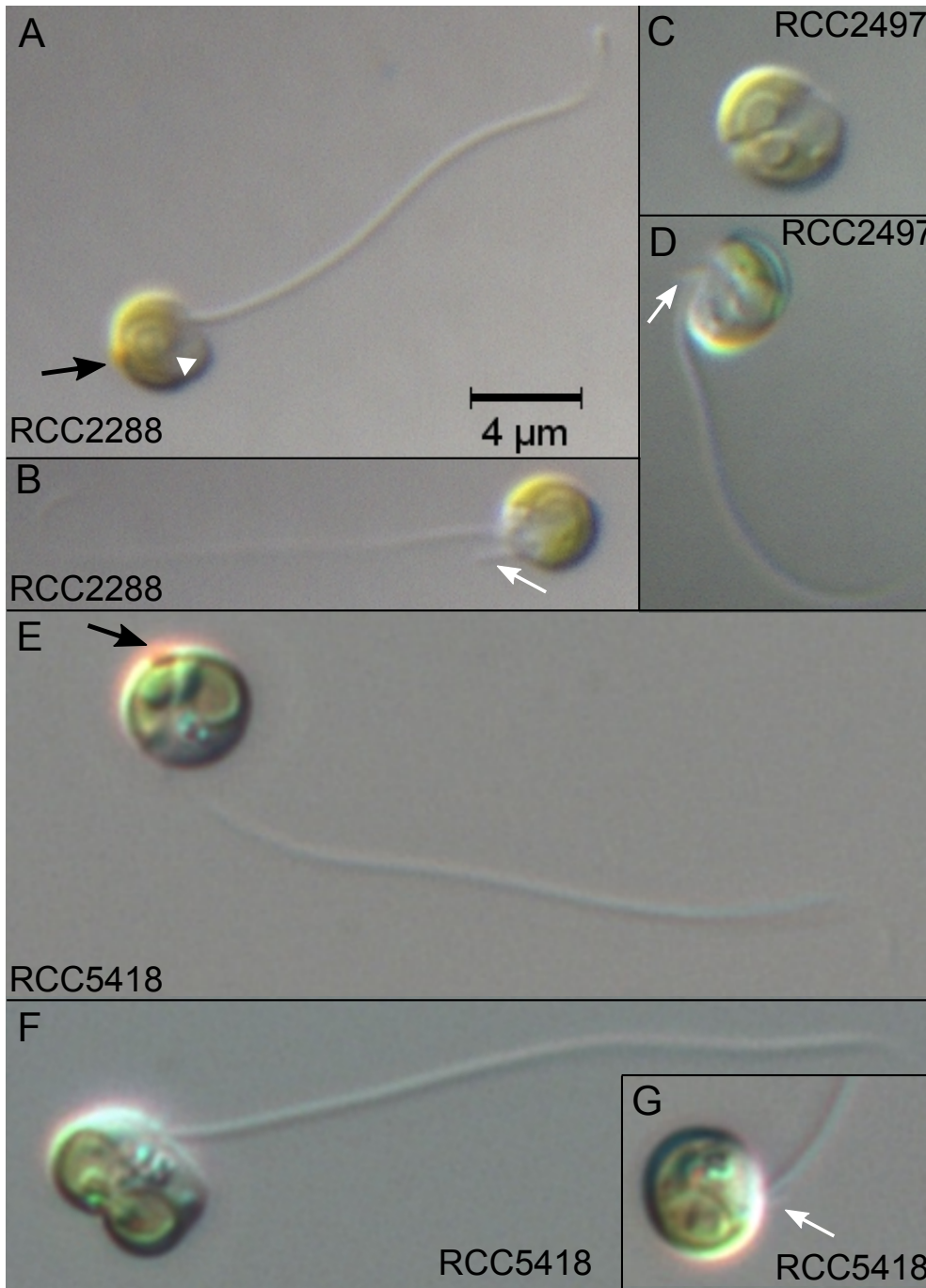
688

689   Figure 3. Light microscopy images of the new *Mantoniella* strains. All strains have round cell

690   morphology, visible red stigma (black arrow), a long and short flagellum (white arrow) and one

691   chloroplast with a pyrenoid (white arrowhead). Scale bar is 4 µm for all images. (**A**–**B**)

692   *M. beaufortii* RCC2288. (**C**–**D**) *M. beaufortii* RCC2497 during cell division and single cell

693   showing long and short flagellum. (**E**–**G**) *M. baffinensis* RCC5418 single cell (**E**), during cell

694   division (**F**) and cell showing the short flagellum (**G** inset).
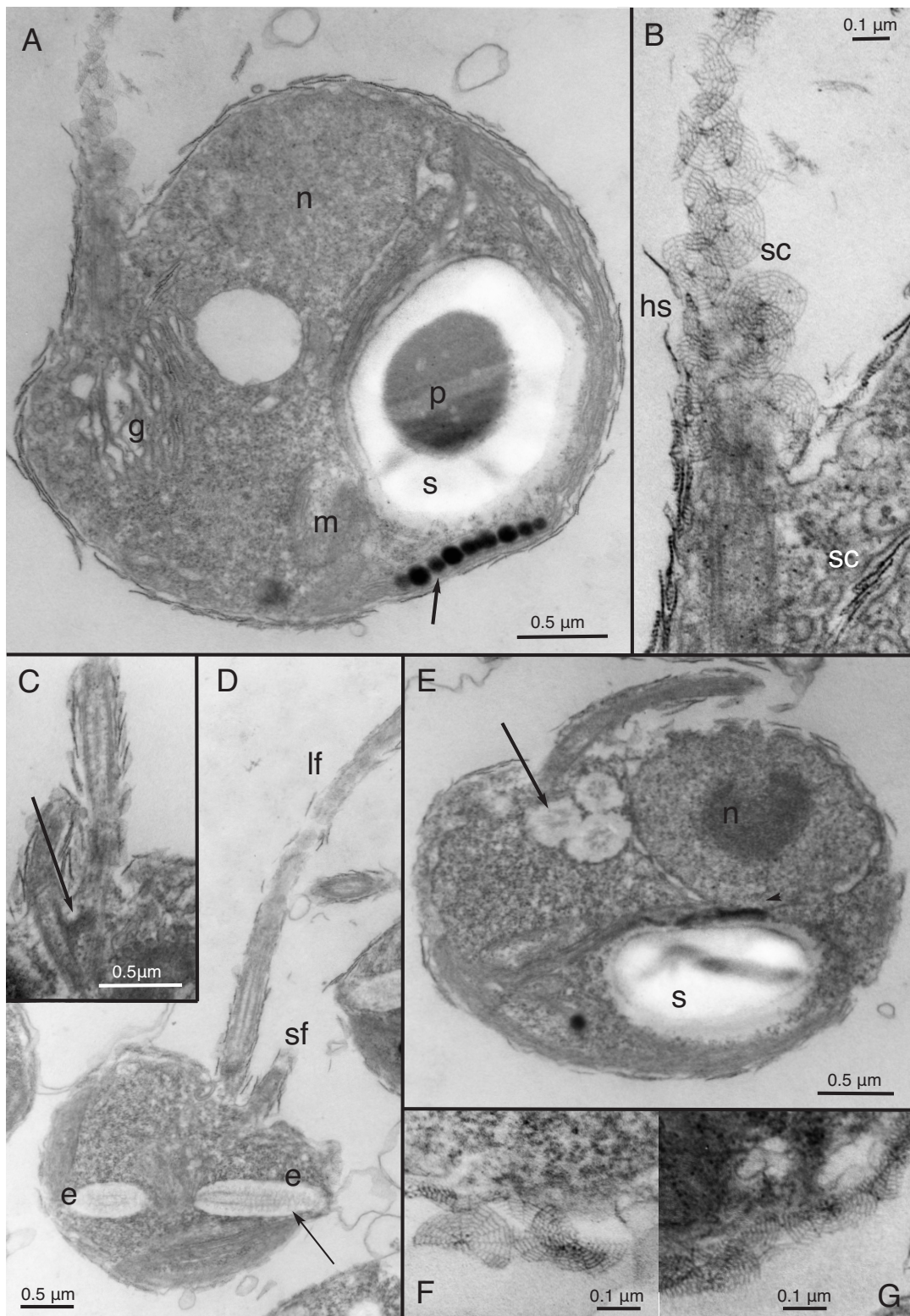
696   Figure 4. TEM thin sections of *M. beaufortii* RCC2288. (**A**) Internal cell structure showing

697   organelles and stigma (black arrow). (**B**) Detail of the hair and spiderweb scales covering the

698   long flagellum. Scales produced in the Golgi body. (**C**) Detail of the flagellar base (black arrow).

699   (**D**) Cell with long and short flagella and longitudinal section of the ejectosomes (black arrow).

700   (**E**) Cross section of ejectosomes (black arrow). (**F**) and (**G**) body scales made up of radiating

701   and concentric ribs. Abbreviations: e=ejectosome, g=Golgi, s=starch granule, m=mitochondrion,

702   n=nucleus, p=pyrenoid, hs=hair scale, sc=scale, lf=long flagellum and sf=short flagellum.
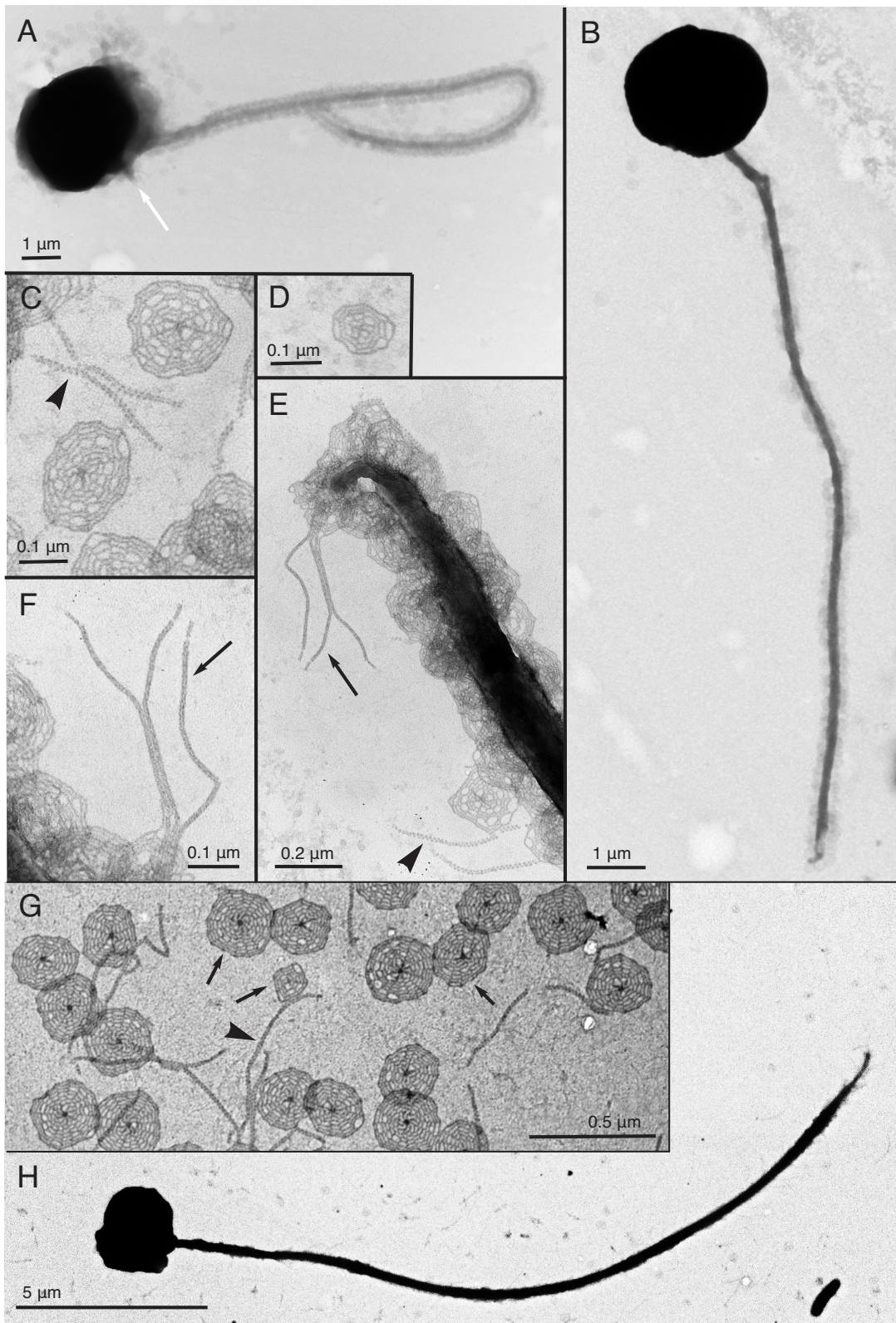
704 Figure 5. Transmission electron micrographs of whole-mounts of the new *Mantoniella* strains.

705 (**A**–**E**) *M. beaufortii.* (**A**) Whole cells of strain RCC2288, indicating the short flagellum (white

706 arrow), and (**B**) RCC2497. (**C**) Detached flagellar spiderweb-like scales and hair scales (black

707 arrowhead). (**D**) Detail of small tetraradial body scale. (**E**) Imbricated scales and hair scales

708 covering the long flagellum. A tuft of three hair scales on the tip of the long flagellum (black

709 arrow) (**F**) Detail of the tuft of hair scales (black arrow). (**G**–**H**) *M. baffinensis* RCC5418. (**G**)

710 Small and large body scales (black arrows) and flagellar hair scales (black arrowhead) and (**H**)

711 whole cell.

712
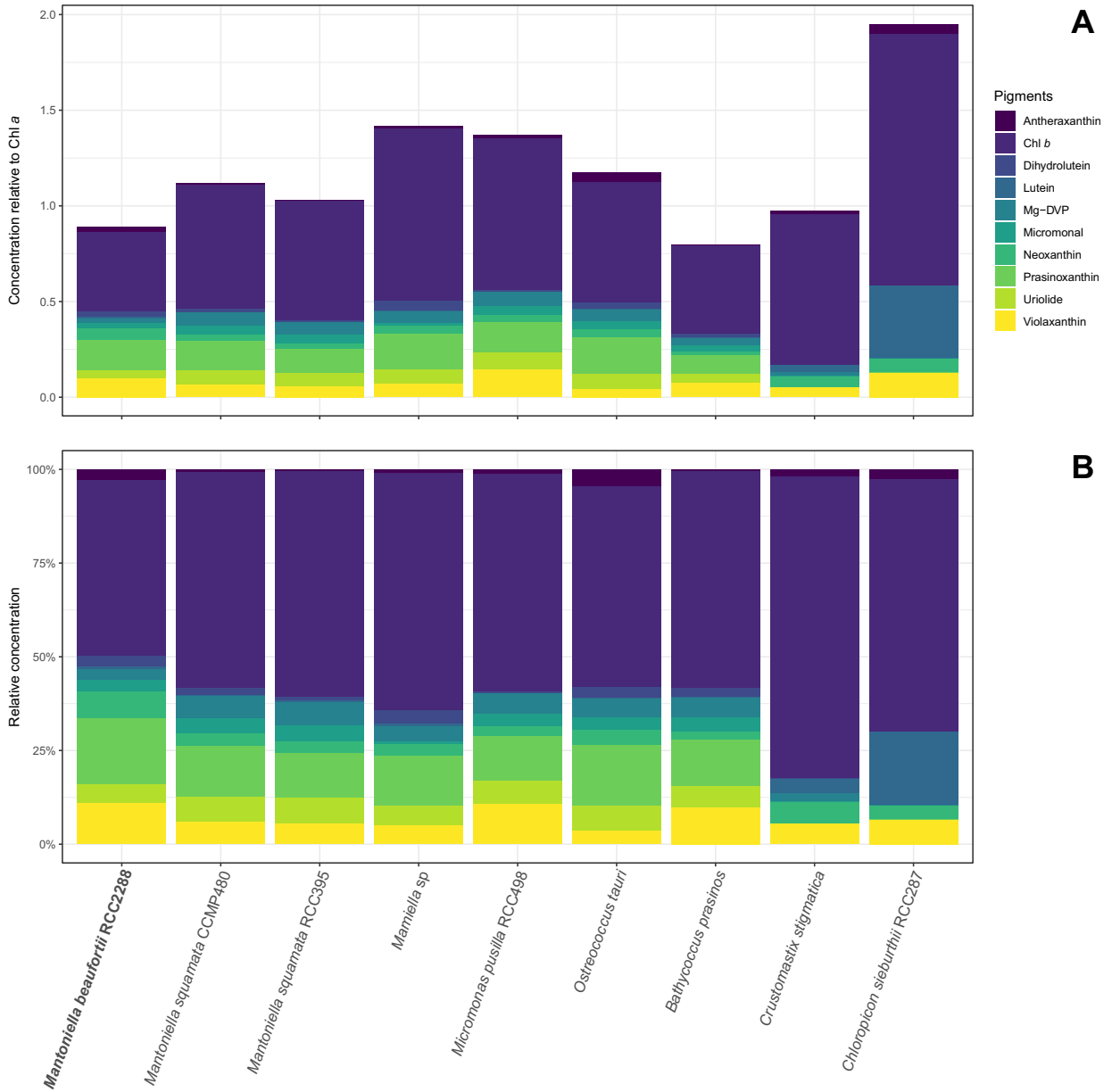
Figure 6. Pigment to chlorophyll *a* ratios in *M. beaufortii* RCC2288 (this study) compared to

other Mamiellophyceae species (data from Latasa et al. 2004). (**A**) Cumulative pigment to

Chlorophyll *a* ratio of Chlorophyll *b* and abundant carotenoids (excluding α- and β-carotene).

(**B**) As for **A**, but showing relative abundances. Mg-DVP: Mg-24-divinyl pheoporphyrin *a*5

monomethyl ester.

718

719
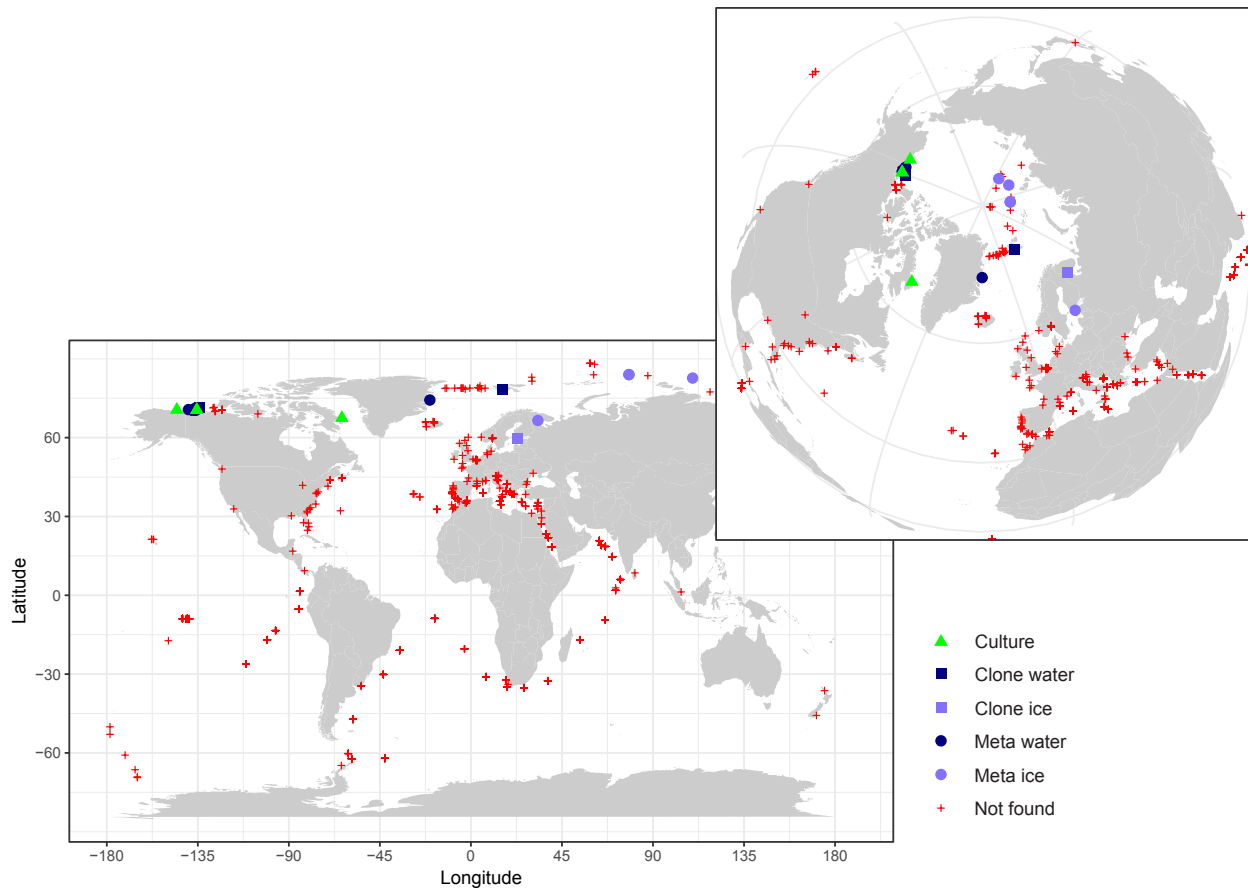
Figure 7. Map of the distribution of *M. beaufortii* in environmental sequence datasets

highlighting its prevalence in Arctic samples (inset). The isolation sites of *M. beaufortii* cultures,

presence of its 18S rRNA gene sequence in clone libraries (Clone water, Clone ice) and

metabarcodes from seawater and ice samples (Meta water, Meta ice) and absence in

metabarcodes (Not found) are plotted. For *M. baffinensis*, only its isolation site is indicated in

Baffin Bay since no similar environmental sequence was found in the datasets analyzed.

Metabarcoding datasets include Ocean Sampling Day, Tara Oceans and polar projects. See

Supplementary Table 2 for a full description of the metabarcoding datasets screened.

728

729

730

732 Table 1. Strains used in this study. RCC: Roscoff Culture Collection (www.roscoff-culture-

733 collection.org). 18S rRNA and ITS show Genbank accession numbers. Strains in bold used to

734 describe the new species.

Strain	Strain Name	Oceanic Region	Latitude	Longitude	Depth of Isolation (m)	18S rRNA	ITS	Remark
RCC2285	MALINA E43.N1	Beaufort Sea	70° 34' N	145° 24' W	0	JF794 053	JQ413368	strain lost
RCC2288	MALINA E47.P2	Beaufort Sea	70° 30' N	135° 30' W	0	JN934 679	JQ413369	
RCC2497	MALINA E47.P1	Beaufort Sea	70° 30' N	135° 30' W	0	KT860 921	JQ413370	
RCC5418	GE_IP_IC_DIL_490	Baffin Bay	67° 28' N	63° 46' W	surface ice	MH51 6003	MH542162	

735

736 Table 2. Cell diameter and long flagellum lengths measured for *M. beaufortii* (RCC2288 and

737 RCC2497) and *M. baffinensis* (RCC5418). n = number of cells measured and SD = standard

738 deviation.

Strain	min	max	mean	median	stdev	n
Cell diameter (µm)						
RCC2288	2.89	4.98	3.77	3.70	0.41	60
RCC2497	3.15	4.74	3.87	3.77	0.39	39
RCC5418	3.54	5.69	4.66	4.66	0.51	69
Long flagellum length (µm)						
RCC2288	12.93	21.47	16.27	15.99	2.63	11
RCC2497	11.91	21.25	16.31	17.07	2.71	12
RCC5418	11.27	32.59	21.78	21.29	5.14	25

739

740 Table 3. Comparison of *Mantoniella* spp. scale types.

Species	Flagellar scales	Body scales
Mantoniella squamata	spiderweb-like heptaradial	spiderweb-like large octoaradial and small rare tetraradial
Mantoniella antarctica	lace-like heptaradial	lace-like hexaradial and smaller heptaradial
Mantoniella beaufortii	spiderweb-like hexaradial	spiderweb-like large heptaradial and small rare tetraradial
Mantoniella baffinensis	spiderweb-like heptaradial	spiderweb-like large octoaradial and small rare tetraradial

741

Supplementary Figures

Supplementary Figure 1. Alignment of the 18S rRNA gene V4 hypervariable region from

M. beaufortii and *M. baffinensis* strains (Red and Orange, respectively), environmental clones

(Blue) and metabarcodes (Green) with a selection of sequences from closely related

Mamiellophyceae. Sequence signatures diagnostic of the two new species are indicated by boxes.

The A region is specific of both species while the B and C regions differ between the two

species.

753

754

755 Supplementary Figure 2. Alignment of the 18S rRNA gene V9 hypervariable region from

756 *M. beaufortii* and *M. baffinensis* strains (Red and Orange, respectively) and environmental

757 clones (blue) with a selection of closely related Mamiellophyceae sequences. Sequence

758 signatures diagnostic of *M. beaufortii* and *M. baffinensis* are indicated by arrows.

759

760
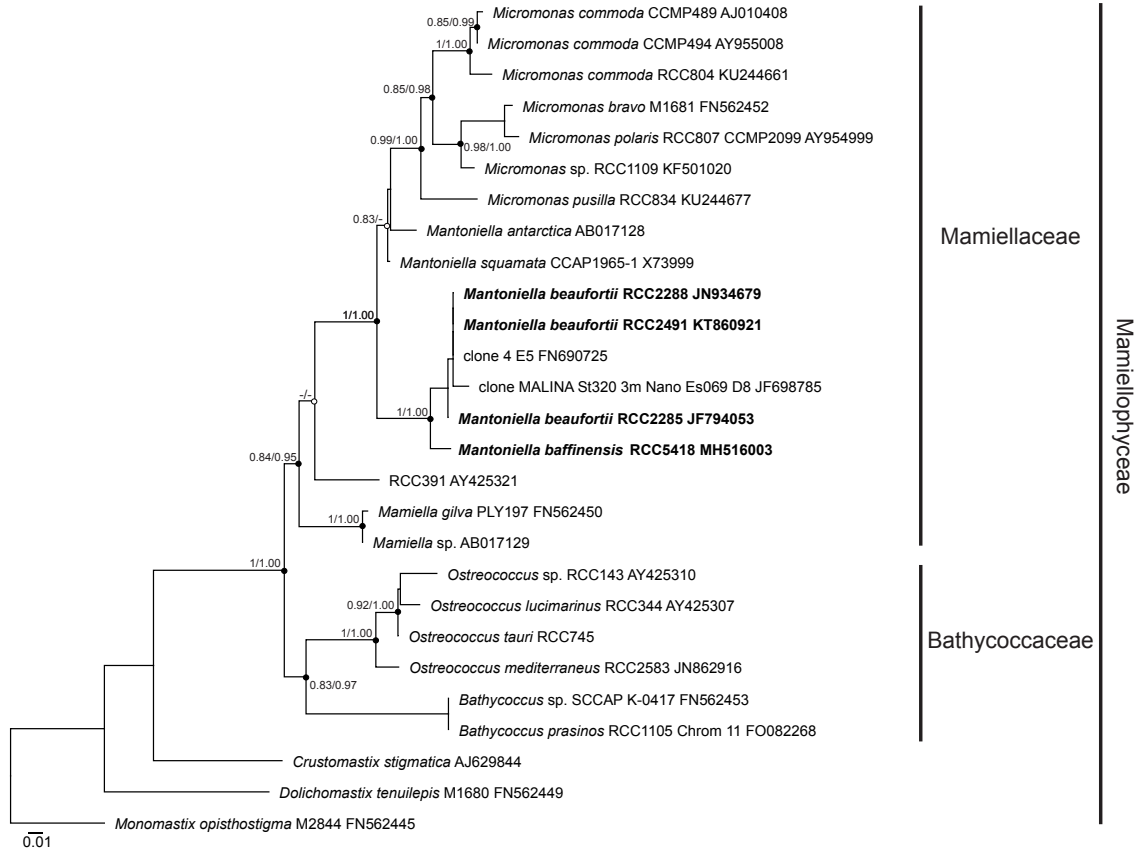
761

762 Supplementary Figure 3. Maximum-likelihood phylogenetic tree inferred from nuclear 18S

763 rRNA sequences of Mamiellophyceae. *Monomastix opisthostigma* was used as an outgroup.

764 Solid dots correspond to nodes with significant support (> 0.8) for ML analysis and Bayesian

765 analysis (>0.95). Empty dots correspond to nodes with non-significant support for either ML or

766 Bayesian analysis, or both. GenBank accessions of the 18S rRNA sequences shown after the

767 species name.

768
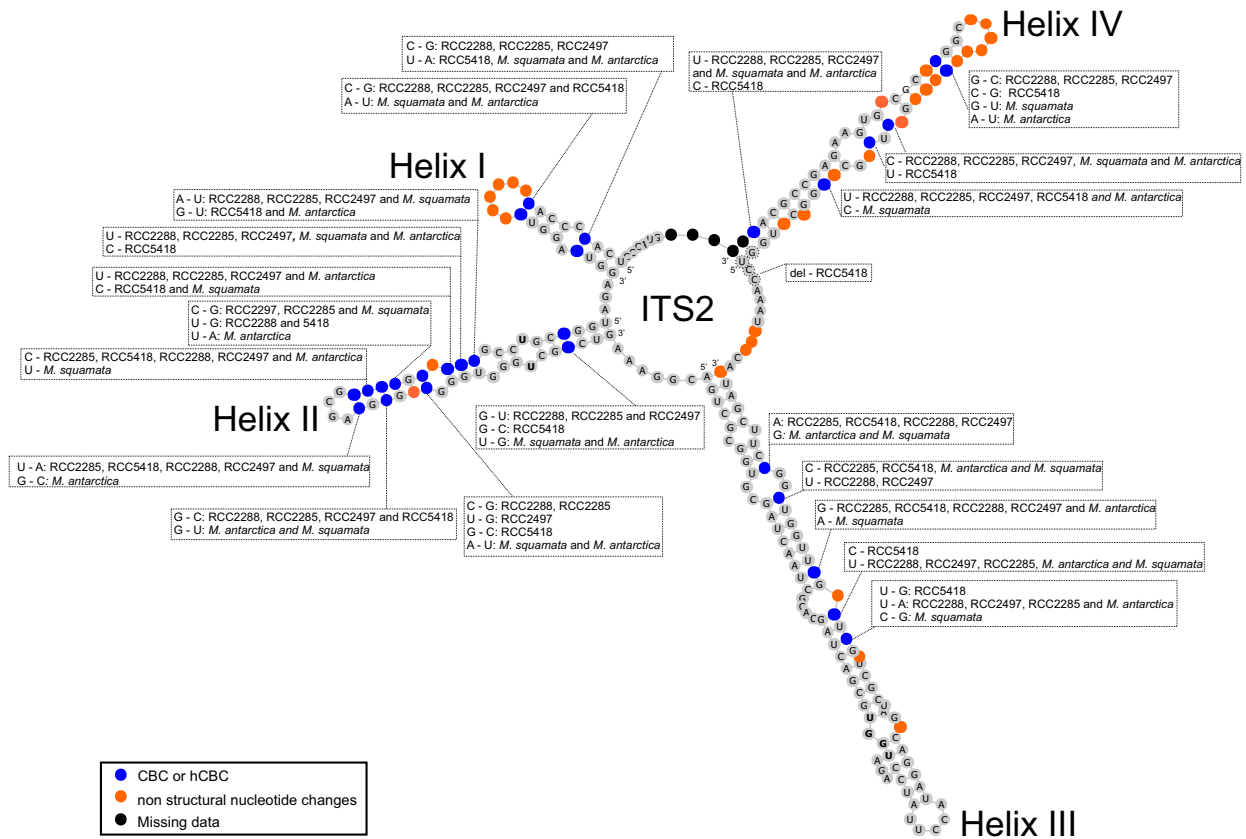
Supplementary Figure 4. Intramolecular folding pattern of the ITS2 molecule of *Mantoniella*

(RCC2288, RCC2285, RCC2497 and RCC5418). The four major helices are labeled as Helix I –

Helix IV. Blue dots represent either CBCs or hCBCs. Non-CBCs (N – N ↔ N × N) are

represented in orange.

774

47
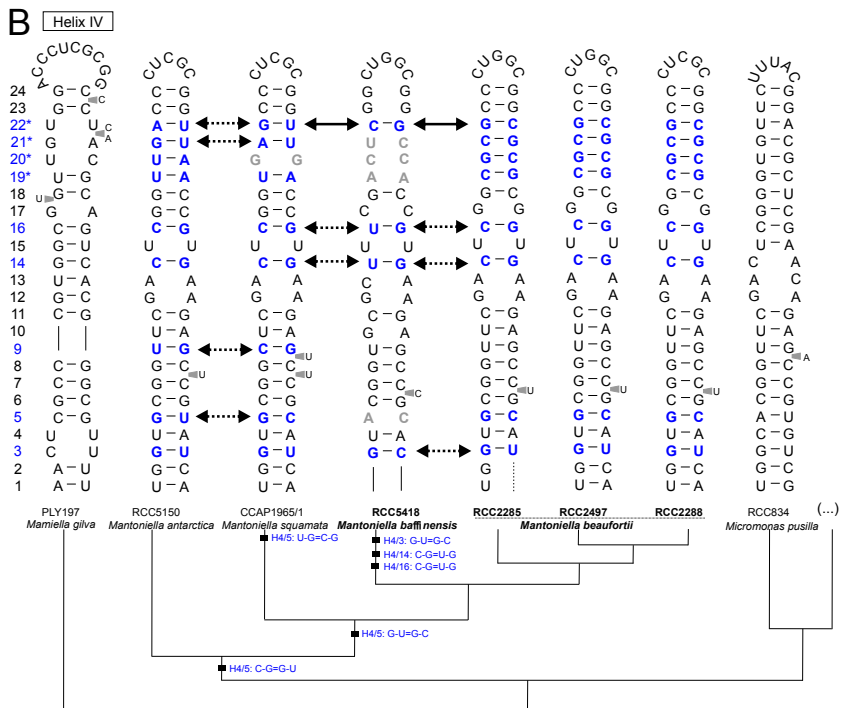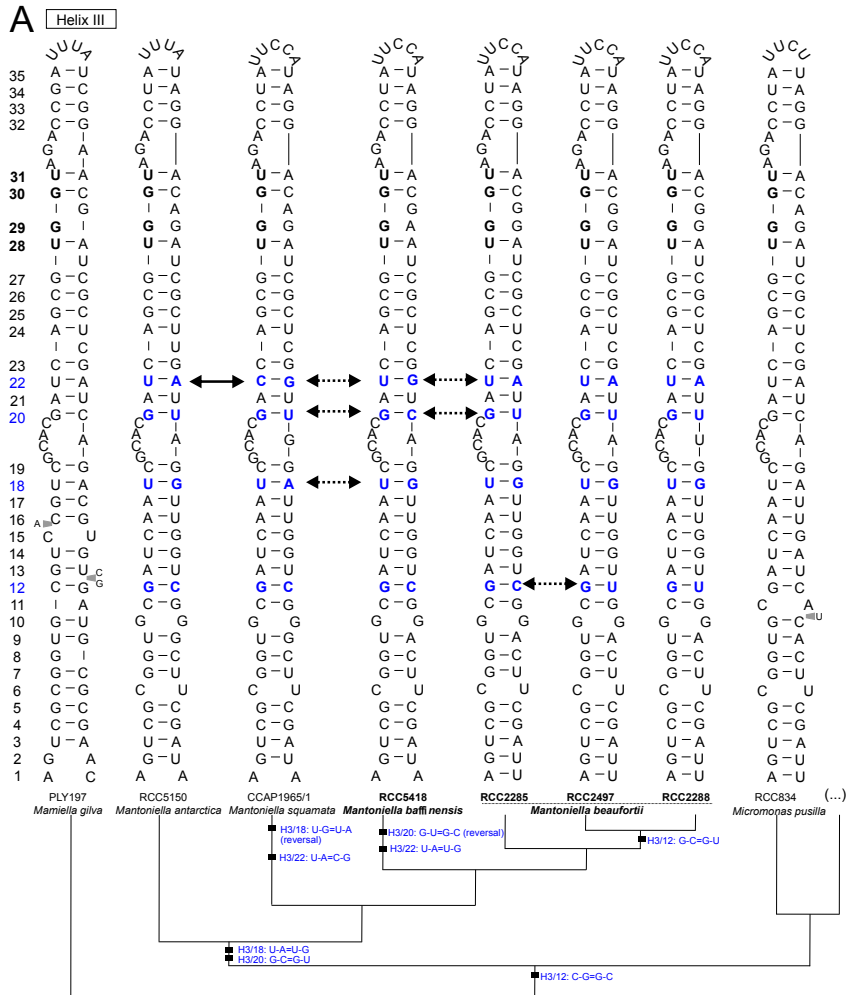
775 Supplementary Figure 5. Molecular signatures of *Mantoniella* species revealed by comparison of

776 ITS2 secondary structures within Mamiellaceae. Signatures in Helix III are shown in (**A**) and

777 Helix IV in (**B**). The conserved base pairs among the different groups are numbered. CBCs and

778 hCBCs are highlighted by solid and dotted arrows, respectively. Hypervariable positions are

779 marked by an asterisk (*). Ellipsis (…) represent the other clades and species of *Micromonas*.

780 The YRRY (pyrimidine-purine-pyrimidine) motif on the 5' side arm of Helix III is shown in

781 bold black. Single nucleotide substitutions are shown by grey nucleotides. Identified

782 homoplasious changes are shown as parallelisms and reversals.

783

784 *Supplementary Tables*

785

786 Supplementary Table 1. Primers and PCR conditions used in this study. Abbreviations: fwd - forward, rev. - reverse, temp -

787 temperature.

Gene	Primer fwd	Sequence 5'-3'	Primer rev.	Sequence 5'-3'	Reference	cycles	Initial time	Denaturation temp	time	temp	Annealing time	temp	Extension time	temp	Elongation time	temp
18S rRNA	Euk63F	ACGCTTGT CTCAAAGA TTA	Euk1818R	ACGGAAA CCTTGTTA CGA	Lepère et al. 2011	35	5 min	95ºC	30 sec	95ºC	30 sec	55ºC	1 min 30 sec	72ºC	10 min	72ºC
ITS1-5.8S-ITS2	329f	GTGAACCT GCRGAAGG ATCA	D1R-R	TATGCTTA AATTCAGC GGGT	Balzano et al. 2017	35	5 min	95ºC	1 min	95ºC	45 sec	55ºC	1 min 15 sec	72ºC	7 min	72ºC

788　Supplementary Table 2. Metabarcoding datasets of the 18S rRNA gene analyzed in this study for

789　the presence of *M. beaufortii* and *M. baffinensis* signatures.

Data set	18S region	Region	Samples	Bioproject or link	Sequencer	Clustering	Reference
Tara Oceans	V9	Oceanic	334	http://doi.pangaea.de/10.1594/PANGAEA.843022	Illumina	Swarm	de Vargas, C., Audic, S., Henry, N., Decelle, J., Mahe, F., Logares, R., et al. (2015). Eukaryotic plankton diversity in the sunlit ocean. Science 348, 1261605. doi:10.1126/science.1261605.
OSD - LGC - 2014	V4	Coastal	157	PRJEB8682	Illumina	0.97	Kopf, A., Bicak, M., Kottmann, R., Schnetzer, J., Kostadinov, I., Lehmann, K., Fernandez-Guerra, A. et al. 2015. The ocean sampling day consortium. Gigascience. 4:27.
MALINA - Monier - 2014	V4	Arctic Ocean	24	PRJNA202104	454	0.98	Monier, A., Terrado, R., Thaler, M., Comeau, A., Medrinal, E. & Lovejoy, C. 2013. Upper Arctic Ocean water masses harbor distinct communities of heterotrophic flagellates. Biogeosciences. 10:4273–86. Monier, A., Comte, J., Babin, M., Forest, A., Matsuoka, A. & Lovejoy, C. 2014. Oceanographic structure drives the assembly processes of microbial eukaryotic communities. ISME J. 9:990–1002.
ACME - Comeau - 2011	V4	Arctic Ocean	11	SRA029114	454	0.98	Comeau, A. M., Li, W. K. W., Tremblay, J.-É., Carmack, E. C. & Lovejoy, C. Arctic Ocean microbial community structure before and after the 2007 record sea ice minimum. PLoS One 6, e27492 (2011)
Nansen Basin - Metfies - 2016	V4	Arctic Ocean	17	PRJEB11449	454	0.97	Metfies, K., von Appen, W.-J., Kilias, E., Nicolaus, A. & Nöthig, E.-M. Biogeography and Photosynthetic Biomass of Arctic Marine Pico-Eukaroytes during Summer of the Record Sea Ice Minimum 2012. PLoS One 11, 20 pp. (2016)
Southern Ocean - Wolf - 2014	V4	Southern Ocean	6	PRJNA176875	454	0.97	Wolf, C., Frickenhaus, S., Kilias, E. S., Peeken, I. & Metfies, K. Protist community composition in the Pacific sector of the Southern Ocean during austral summer 2010. Polar Biol. 37, 375–389 (2014)
Fieldes Bay - Luo - 2016	V4	Southern Ocean	10	PRJNA254097	Illumina	0.97	Luo, W. et al. Molecular diversity of microbial eukaryotes in sea water from Fildes Peninsula, King George Island, Antarctica. Polar Biol. (2015). doi:10.1007/s00300-015-1815-8
Fram Strait - Kilias - 2013	V4	Arctic Ocean	5		454	0.97	Kilias, E., Wolf, C., Nöthig, E.-M., Peeken, I. & Metfies, K. Protist distribution in the Western Fram Strait in summer 2010 based on 454-pyrosequencing of 18S rDNA. J. Phycol. 49, 996–1010 (2013).

790

791

792

793

794

795

796

797

798

799

800

801

802 Supplementary Table 3. Morphological characters in Mamiellophyceae species.

Species	Flagella	Spider web-like scales	Circular patterned scales	T-hair scales: tubular shaft	T-hair scales: globular subunits
Bathycoccus prasinos	no	+	-	-	-
Ostreococcus tauri	no	-	-	-	-
Ostreoccoccus mediterraneus	no	-	-	-	-
Mamiella gilva	2 long	+	-	-	+
Mantoniella squamata	1 long, 1 short	+	-	-	+
Mantoniella antarctica	1 long, 1 short	+	-	-	+
Mantoniella beaufortii	1 long, 1 short	+	-	-	+
Mantoniella baffinensis	1 long, 1 short	+	-	-	+
Micromonas pusilla	1 long, 2 extending microtubules	-	-	-	-
Micromonas commoda	1 long, 2 extending microtubules	-	-	-	-
Micromonas polaris	1 long, 2 extending microtubules	-	-	-	-
Micromonas bravo	1 long, 2 extending microtubules	-	-	-	-
Crustomastix didyma	2 long	-	-	+	-
Crustomastix stigmatica	2 long	-	-	+	-
Dolichomastix eurylepidea	2 long	+	-	?	?
Dolichomastix lepidota	2 long	-	-	-	+
Dolichomastix nummulifera	2 long	-	+	?	?
Dolichomastix tenuilepsis	2 long	+	+	+	-

803

804

805

806

807

808

809

810

Supplementary Table 4. Pigment composition of *M. beaufortii* (RCC2288) compared to a

812 selection of green algae. Values are shown as a ratio of pigment to Chl *a* concentration and

813 percent contribution to total carotenoids (in italics). See Supplementary Table 5 for the full

814 names of the pigments.

Species	Order	Phytn a	Chld a	Chl b	Mg-DVP	%	Uri	%	Neo	%	Pra	%	Vio	%	Mmnal	%	Ant	%	Lut	%	Dihy	%	α-car + β-car	%
M. beaufortii RCC2288	Mamiellales	0.006	0.012	0.416	0.024	3.6	0.045	6.6	0.063	9.4	0.156	23.2	0.099	14.6	0.028	4.2	0.025	3.7	0.006	0.9	0.027	4.0	0.167	24.8
M. squamata CCMP480*	Mamiellales	ND	ND	0.644	0.068	10.1	0.075	11.1	0.04	5.5	0.15	22.2	0.068	10.1	0.045	6.7	0.006	0.9	0.003	0.4	0.021	3.1	0.121	17.9
M. squamata RCC395*	Mamiellales	ND	ND	0.62	0.065	12.2	0.073	13.7	0.03	5.8	0.123	23.1	0.056	10.5	0.043	8.1	0.003	0.6	0.004	0.8	0.009	1.7	0.062	11.7
O. tauri RCC116*	Mamiellales	ND	ND	0.633	0.061	8.6	0.079	11.1	0.05	6.3	0.191	26.9	0.044	6.2	0.039	5.5	0.051	7.2	0.003	0.4	0.032	4.5	0.098	13.8
B. prasinos RCC113*	Mamiellales	ND	ND	0.462	0.041	9.7	0.047	11.1	0.02	4.3	0.097	22.9	0.078	18.4	0.03	7.1	0.002	0.5	0.003	0.7	0.018	4.3	0.029	6.9
M. pusilla CCMP490*	Mamiellales	ND	ND	0.768	0.072	9.7	0.096	13.0	0.05	6.1	0.191	25.8	0.103	13.9	0.053	7.2	0.019	2.6	0.006	0.8	0.01	1.3	0.058	7.8
Mamiella sp. RCC391*	Mamiellales	ND	ND	0.896	0.060	8.7	0.072	10.5	0.04	6.3	0.189	27.6	0.074	10.8	0.01	1.5	0.011	1.6	0.008	1.2	0.052	7.6	0.082	12.0
C. stigmatica*	Dolichomastigales	ND	ND	0.786	0.023	3.5	0	0	0.06	8.4	0	0	0.055	8.3	0	0	0.017	2.6	0.038	5.7	0	0	0.305	45.9
C. sieburthii RCC287†	Chloropicales	ND	0.106	0.986	0	0	0	0	0.17	14.8	0	0	0.572	50.8	0	0	0.024	2.1	0.363	32.2	0	0	-	-
P. parkeae CCMP724*	Pyramimonadales	ND	ND	0.677	0.001	0.4	0	0	0	0	0	0	0.077	27.7	0	0	0.002	0.7	0.07	25.2	0	0	0.088	31.7
N. pyriformis CCMP717*	Nephrodelmidaceae	ND	ND	0.698	0.015	3.5	0	0	0.02	5.0	0	0	0.077	18.2	0	0	0.016	3.8	0.022	5.2	0	0	0.065	15.3
Tetraselmis sp. RCC234*	Chlorodendrales	ND	ND	0.812	0.022	4.6	0	0	0.03	6.8	0	0	0.057	11.8	0	0	0.006	1.2	0.096	19.9	0	0	0.082	17.0
P. marina*	Pseudoscourfieldiales	ND	ND	0.871	0.071	13.3	0	0	0.06	10.7	0.287	53.8	0.036	6.8	0	0	0	0	0.003	0.6	0	0	0.033	6.2
P. capsulatus CCMP1192*	Prasinococcales	ND	ND	0.62	0.098	16.7	0.097	16.6	0.08	13.0	0.183	31.2	0.035	6.0	0	0	0.001	0.2	0.015	2.6	0.005	0.9	0.025	4.3

815 *Values from Latasa et al. 2004, †Values from Lopes dos Santos et al. 2016.

816

817

818

819

820

821

822

823

824

825   Supplementary Table 5. Pigments analyzed in this study. LOD, limit of detection.

Pigment	Abbreviation	Retention time (min)	Detection adsorption wavelength (nm)	LOD (ng/inj)	LOD in 1 L filtered (mg.m-3)
Mg-24-divinyl pheoporphyrin *a*5 monomethyl ester	MgDVP	6.3	450	0.015	0.0004
Chlorophyllide *a* and Chlorophyllide *a*-lik	Chld *a* + Chlc	6.3	667	0.016	0.0004
Uriolide	Uri	11.6	450	ND	ND
Neoxanthin	Neo	13.5	450	0.008	0.0002
Prasinoxanthin	Pra	14.0	450	0.008	0.0002
Violaxanthin	Vio	14.3	450	0.010	0.0002
Micromonal	Mmnal	15.0	450	ND	ND
Antheraxanthin	Ant	16.3	450	0.012	0.0004
Unknown carotenoid λmax 412, 436, 46	Unk 1	16.5	450	ND	ND
Unknown carotenoid λmax 452 nm	Unk 2	18.1	450	ND	ND
Lutein	Lut	18.3	450	0.012	0.0002
Dihydrolutein	Dihy	18.6	450	ND	ND
Chlorophyll *b*-degradation product	Chl*b*-deg	22	450	ND	ND
Chlorophyll *b*	Chl *b*	22.4	450	0.004	0.0001
Chlorophyll *b*-like	Chl *b-like*	22.8	450	0.004	0.0001
Chlorophyll a, allomers and epimers	Chl *a*	24.3	667	0.011	0.0002
Phaeophytin *a* and Phaeophytin *a*-like	Phytn *a* + Ph	25.9	667	0.006	0.0002
α-Carotene and β-Carotene	α-car + β-car	26.9	450	0.012	0.0004

826

827